ChemComm

Conductive Two-Dimensional Metal-Organic Frameworks as Multifunctional Materials

Journal:	*ChemComm*
Manuscript ID	CC-FEA-04-2018-002871.R1
Article Type:	Feature Article

ChemComm

FEATURE ARTICLE

Conductive Two-Dimensional Metal-Organic Frameworks as Multifunctional Materials

Michael Ko, Lukasz Mendecki, and Katherine A. Mirica*

Received 00th January 20xx,

Accepted 00th January 20xx

DOI: 10.1039/x0xx00000x

www.rsc.org/

Two-dimensional (2D) conductive metal-organic frameworks (MOFs) have emerged as a unique class of multifunctional 2D materials due to their compositional and structural diversity accessible through bottom-up self-assembly. This feature article summarizes the progress in the development of 2D conductive MOFs with emphasis on synthetic modularity, device integration strategies, and multifunctional behavior. Applications spanning sensing, catalysis, electronics, energy conversion, and storage are discussed. The challenges and future outlook in the context of molecular engineering and practical development of 2D conductive MOFs are addressed.

Introduction

MOFs as a Modular Class of 2D Nanomaterials

The discovery and development of multifunctional two-dimensional (2D) materials, which exhibit exceptional properties—charge transport,[1] large field-effect,[2] and unique light-matter interactions[3]—that are distinct from the bulk, can enable unprecedented approaches to addressing challenges in healthcare, energy conversion, storage, and electronics.[1, 2, 4] Characterized by layered structures, comprising stacked individual sheets held together by intermolecular forces, the thickness of individual layers can vary from one to several atoms, but typically does not exceed 5 nm.[1] Since the pioneering work of Geim and Novoselov on the exfoliation of bulk graphite into graphene,[5] many other types of 2D materials, including transition metal dichalcogenides (e.g., MoS_2, WS_2),[6-9] graphitic carbon nitride,[10, 11] hexagonal boron nitride,[12-14] MXenes,[15] metal oxides,[16, 17] noble metals,[18-20] layered double hydroxides,[21] inorganic perovskites,[22, 23] layered group III-IV semiconductors (e.g., GaSe),[24, 25] metal-organic frameworks (MOFs),[26-28] and black phosphorous (BP)[29, 30] (**Figure 1**), have been obtained and characterized as thin layered nanostructures. The diversity and the unique electronic, physical, and chemical properties of these materials arising from confinement of electronic and magnetic states in two dimensions have given rise to remarkable breakthroughs in environmental,[31-34] healthcare[35, 36] and security applications[37, 38] due to their atomically-thin layered structure,[2] large surface chemical activity,[39-41] high surface-to-volume ratio[42, 43] and large chemical adsorption capacity.[44-46]

The drive to apply the unique features of 2D materials has stimulated the rapid development of numerous synthetic techniques for their preparation.[10, 47-52] The available methods can be subdivided into two distinct categories: bottom-up and top-down approaches.[2] Bottom-up approaches involve building the 2D nanomaterials from the atomic scale by assembling the materials from atoms or molecules, using wet chemical synthesis, chemical vapour deposition (CVD), or physical vapour transport.[2] Top-down techniques typically rely on mechanical exfoliation, chemical etching, or expansion and separation of layers by intercalation.[53] These synthetic routes offer different degrees of control over the size,[54] composition,[10] thickness,[55] crystallinity, and number of defects. The preparation of 2D materials certainly has limitations, but there has been a rapid improvement to overcome the disadvantages.[2]

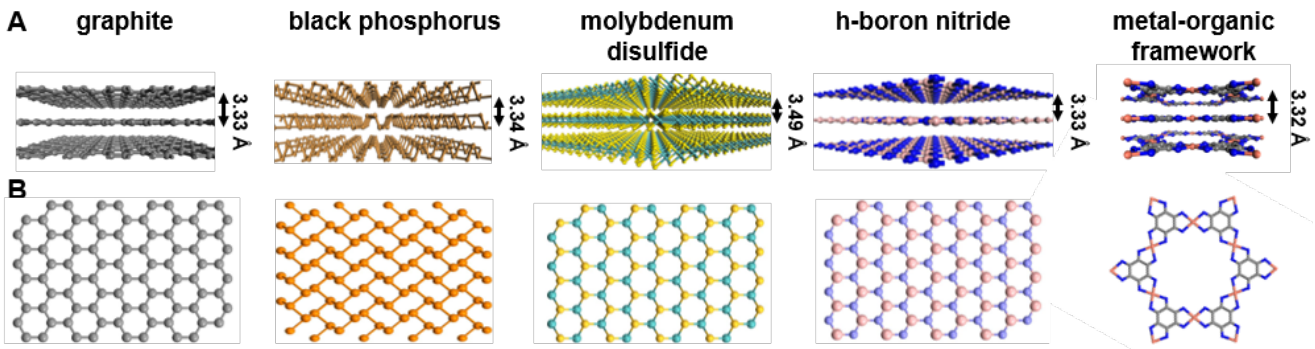

Figure 1. A) A molecular model of representative two-dimensional materials viewing down the c-axis with the interatomic distance between each layer. B) A face-on view of a single layer for each representative material.

In contrast to most 2D materials, 2D MOFs can be formed through self-assembly of molecular building blocks comprising organic linkers and metallic nodes to produce numerous structural possibilities.[56] The resulting materials, characterized by intrinsic permanent porosity and structural rigidity,[57] can provide uniform active sites and open channels for chemo-, shape-, size- and stereoselective interactions. Synergistically coupling these unique structural features with established properties of 2D nanomaterials—tuneable band-gap, charge transport, electrocatalytic activity, double-layer capacitance, and light-matter interactions—can induce intriguing properties in MOFs.[2, 58] The large degree of organisational tunability accessible through solution-phase self-assembly coupled with the potential for multifunctionality set 2D MOFs apart as the new generation of functional 2D materials.

Scope of the review

This article focuses on highlighting the latest fundamental and applied advances in research on layered conductive MOFs, as an emerging class of multifunctional 2D materials. We discuss the unique electrical properties of 2D conductive MOFs as a function of their molecular composition and structure. We also review several key methods available for integrating MOFs into devices and summarize recent progress in the application of 2D conductive MOFs for the development of sensing devices, electrocatalysts, energy storage devices, and transducers. We conclude by pointing out existing gaps in fundamental understanding and offering a perspective on the future potential applications of 2D conductive MOFs.

Principles of electrical conductivity in 2D MOFs

The development of crystalline and porous metal-organic frameworks (MOFs) through the molecular self-assembly of inorganic metallic nodes with organic linkers has revolutionized access to modular solid-state materials.[59-61] The strategic selection of tuneable molecular building blocks, has provided a remarkable variety of MOF-based solid-state structures with diverse utility in catalysis,[62, 63] gas storage,[64] energy,[65, 66] and chemical sensing.[67, 68, 58] Until recently, the ability to harness and actuate this utility within electronic and electrochemical devices has been limited due to the inherently low electrical conductivity of most MOFs.[69, 70]

Achieving electrical conductivity in solid-state materials requires maximizing the concentration and mobility of charge carriers.[70, 71] Due to the hybrid organic-inorganic character and structural modularity of MOFs, engendering electrical conductivity in these materials offers the opportunity to capitalize upon and integrate the general principles of molecular engineering of at least four classes of materials: 1) conductive organic polymers,[72-74] 2) conductive organic molecular solids,[75-77] 3) conductive coordination polymers,[78, 79] and 4) elemental (e.g., Si, Ge) and inorganic semiconductors (e.g., CdSe, InAs).[5, 80-83] The generation of charge carriers in MOFs can be achieved by i) thermal or photo-excitation,[84-86] ii) doping,[86-88] and iii) hole or electron injection,[86-88] while mobility can be maximized by i) lowering the defect density in the material,[89] ii) reducing the number of charge trapping sites,[89, 90] and iii) minimizing grain boundaries.[91] Hendon et al. have proposed several approaches that can harness established principles of hopping, through-space, through-bond, and band transport in known semiconductors.[92] Recent perspectives and reviews[58, 70, 93] have summarized structural features and design principles that can enable the experimental realization of electrical transport in MOF-based materials.[58, 93-95]

Initial approaches towards obtaining conductive MOFs have relied on post-synthetic introduction of external guest molecules that promote through-bond charge transport by acting as bridges between the neighbouring molecular building blocks that compose a MOF.[66] Integration of redox-active guests (e.g., TCNQ) has also proven to be an effective strategy for achieving charge transport through the host-guest charge transfer interactions.[96, 97] For instance, Talin et al. demonstrated that through soaking the $Cu_3(BTC)_2$ MOF (benzene-1,3,5-tricarboxylic acid) in TCNQ solution, the conductivity of this MOF can be altered from 10^{-8} S cm^{-1} to 0.07 S cm^{-1}, further demonstrating that doping strategies can be readily employed to enhance electrical conductivity of 3D MOFs.[69] More recently, Allen et al. incorporated a series of cross-linked benzene dicarboxylic acid (bdc) derivatives into the isoreticular lattice of MOFs.[98] Although the cross-linked MOFs were not conductive, this experimental approach can offer a potential alternative to install conductive pathways for a wide range of MOF topologies.

The drawbacks of doping-based approaches, however, may lead to the decreased surface area, porosity, and pore volume due to pore occlusion by incorporated guest molecules, limited thermal stability, and tendency to phase separate the guest molecule from the material under conditions to synthesize MOF monolayers, all of which may be undesirable for refined control of structure-property correlations.[58, 69] Therefore, molecularly homogeneous and inherently electrically conductive MOFs are highly desirable as multifunctional materials. Recent development of MOFs with substantial electrical conductivity through the strategic selection of molecular building blocks that utilize planar, conjugated, and redox active organic linkers have made it possible to harness unique characteristics of MOFs, such as porosity for gas uptake, catalytically-active sites, and tailored host-guest interactions within electronic devices.[99]

Intrinsically conductive MOFs display conduction mechanisms consistent with those of organic and inorganic semiconductors including hopping (**Figure 2A**),[71, 100, 101] through-space (**Figure 2B**),[102, 103] through-bond (**Figure 2C**),[104, 105] and band transport.[106, 107] Hopping conduction relies on the charge movement from the donor to the acceptor molecules.[101, 108, 109] There are localized states of charges with discrete energy levels that reside on specific sites, and under favourable conditions (e.g., spatial distance, and energy difference) the charge carriers can hop between neighbouring units.[70, 108-110] Hopping mechanism have been identified in M_2(DEBDC) MOF (M = Mn^{2+}, Fe^{2+}; E = O, S) and Fe-MOF-74.[111, 112] Through-space conduction is similar to the hopping mechanism, and depends on the transport of charge carriers between the donor and acceptor sites in the material.[113, 114] Non-covalent interactions (e.g., π-π) can provide direct spatial and orbital overlap to

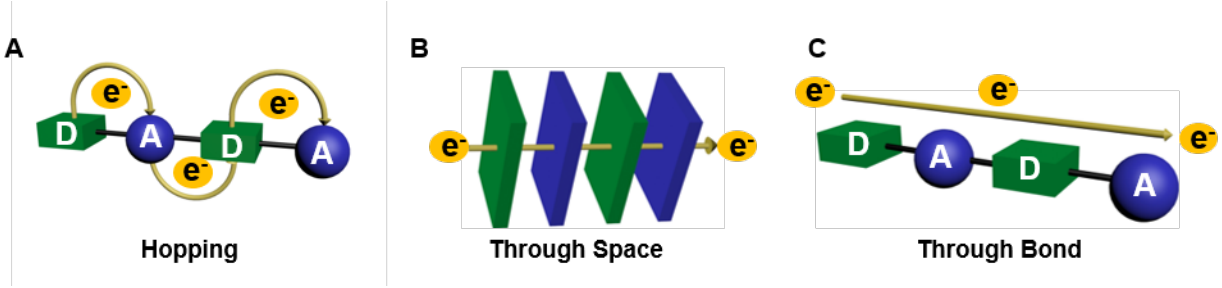

Figure 2. Representation of possible modes of charge transport in 2D MOFs such as A) hopping charge transport, B) through-space charge transport, and C) through-bond charge transport.

induce through-space charge transport.[70, 115] Through-space charge transport due to π-π interactions was shown in tetrathiafulvalene (TTF) and anthraquinone disulfonate based MOFs.[102, 103, 116] The through-bond conduction relies on the movement of charge carriers through continuous coordination or covalent bonds in the conductive material.[117, 118] This mechanism is strongly influenced by the orbital symmetry, and energy level overlap between the metal node and organic linker). Through-bond conduction was shown in $Cu[Cu(pdt)_2]$ (pdt=2,3-pyrazinedithiolate) MOF interconnected with copper bis(dithiolene) units.[104] Band transport mechanism relies on the delocalization of the charge carriers through the valence or conduction band.[119, 120] The overall charge mobility is dictated by effective mass of the charge carriers and the extent of charge scattering in the material.[70, 110]. The tunability of the band gap in isoreticular $M_3S_6C_6$ (M = Mg, Ca, Zn, Cd, Ge, and Sn) MOFs has been recently assessed by Deng and co-workers using first principle calculations.[121] The authors found that the effective mass of the charge carriers is significantly influenced by the metal *d* band.[121] As the coupling between *p-d* orbitals of the metal and organic linker increases, the effective mass of charge carriers decreases and gives rise to enhanced conduction.[119, 121]

Planar MOFs with extended 2D π-conjugation and graphene-like structures are currently among the most conductive frameworks known.[122-125] The confinement of charge carriers within the 2D lattice forces charge transport in the direction of the plane due to improved conjugation and enhanced *p-d* orbital coupling.[2, 58, 70, 92, 126, 127] In 2D conductive MOFs, both metallic nodes and organic linkers can serve as the source of charge carriers.[58, 70, 127] More specifically, organic linkers with either stable radicals or redox active molecules together with the metal centres possessing unpaired electrons can be employed to ensure high charge delocalization through continuous conjugation in the MOF.[95] While the specific mechanism of charge transport through 2D porous MOF networks is not yet well-understood, strategies to synthesize 2D conductive MOFs can be drawn from semiconductors and 3D MOFs.[70, 93] Since hopping, through-space, through-bond, and band transport conduction mechanisms require good spatial and energetic overlap between the orbitals of appropriate symmetry, the electronic structure of conductive MOFs can be thus modulated by the design of organic linkers, and the choice of incorporated metals that offer good charge delocalization through the material.[58, 59, 70, 92] For instance, the orbitals of the metal in the MOF framework may form either the upper valence or lower conduction band of the MOF. Therefore, depending on charge state and the identity of metallic nodes, metal substitution can affect oxidation (hole injection) and reduction (electron injection) processes within the material, and therefore influence its electronic properties.[128]

Conventional push-pull strategies relying on the electron-donating or electron-withdrawing nature of additional substituents can be employed to modulate the electron density and delocalization of the organic ligands comprising the MOFs. For instance, the incorporation of primary amines onto the benzene-based building block will increase the electron-density on this organic linker.[129] Another approach may involve the use of inherently redox-active ligands that exhibit numerous accessible redox states, such as 2,3,6,7,10,11-hexahydroxytriphenylene.[68, 123, 130-132] In the case of Ni_3HITP_2, the highly π-stacked and extended π-conjugated network enables high electrical conductivity.[133]

Initial studies by Dincă and co-workers[122] showed that bulk multi-layered Ni_3HITP_2 behaves as a semiconductor whereas computational studies by Zeng and co-workers[134] calculated the bulk multi-layered material to possess metallic conductivity. By replacing the Ni metal centre to Cu forming Cu_3HITP_2, the theoretical calculations maintained metallic conductivity.[134] Interestingly, the calculations on 2D sheets reported a change in conductivity from metallic to semiconducting for Ni_3HITP_2 while Cu_3HITP_2 remained the same.[134] Although the 2D sheet for Ni_3HITP_2 is predicted to be semiconducting, novel strategies need to be developed for modulating the structure to achieve controlled semiconducting properties. Electronic structure calculations showed that increasing interlayer spacing or layer-by-layer displacement can induce changes in band structure.[133] The disconnect between theoretical calculations and experimental analysis may arise from the presence of transport barriers in experimental systems (e.g., interfaces and defects), that are not present in computational models.[133] There are three potential defects that play a role in charge transport which are perpendicular grain boundaries, strike-slip faults between grains, and layer-layer displacements.[133] As described by Talin and co-workers, introducing transport barriers in computational work provides a plausible explanation for the disagreement between theoretical and experimental work.[133]

Structural features and preparation strategies of 2D conductive MOFs

Established strategies for constructing 2D conductive MOFs rely on square planar or octahedral transition metal ions (Cu, Ni,

Co, and Pd) crosslinked with flat, conjugated (e.g., benzene, triphenylene or phthalocyanine-based) ligands containing ortho-substituted hetero atoms (O, S or NH) (**Figure 3**).[70] The symmetric structure of the ligand typically determines the resulting structure and the shape of the pores within the MOF. The most common method for producing MOFs is solvothermal synthesis.[135] The core building block components—the metal node in the form of a metal salt and the organic linker —are placed into an appropriate solvent, and heated. The MOF solid is then filtered, and washed to remove residual reagents or biproducts.[136]

Subtle changes in the molecular substitution of the ligand and the choice of the metal node can dramatically influence the stacking mode and the presence of structural defects within layered MOFs. The chemical identity of the crosslinking

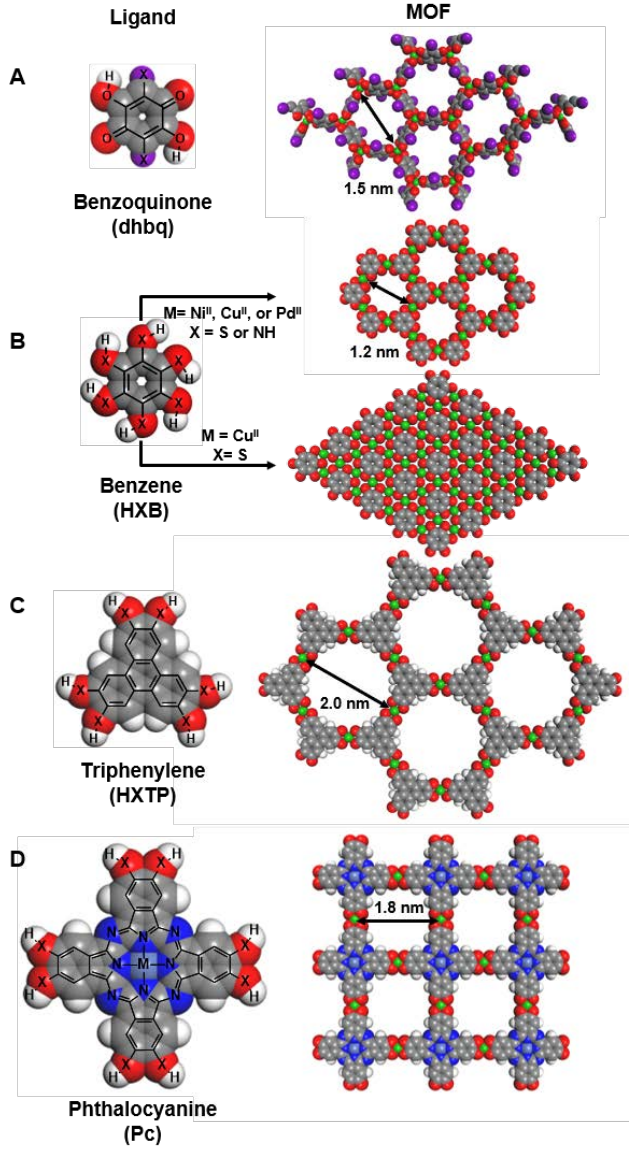

Figure 3. Core organic ligand building blocks for the construction of 2D MOFs. Different ligands lead to the formation of specific MOF topologies which vary in the pore size and shape. A) Benzoquinone ligands form non-planar 2D MOFs.[137] B) Benzene or triphenylene based ligands form no pore or hexagonal pores with sizes ranging from 1.2-2.0 nm.[138] C) Triphenylene ligands form MOFs with the largest pore size for 2D MOFs.[123, 125, 139, 140] D) Phthalocyanine ligands form square pore shapes with an opening of 1.6 nm.[141]

heteroatom (e.g., O, S, NH) in combination with the choice of the metal node, together have a substantial effect on the stacking mode (e.g., slipped parallel, eclipsed, or staggered) and pore diameter of the MOF based on the general structure of the hexasubstituted triphenylene (**Figure 4**). For example, a Cu^{II} metal salt reacting with hexahydroxytriphenylene (HHTP) forms a MOF that stacks in a slipped parallel mode of the extended interconnected layer in an AAAA pattern (**Figure 4A, top**). Altering the metal salt to Ni^{II} or Co^{II} drastically changes the structure of the material under similar synthetic conditions. The structural analysis of the single crystal of Co_3HHTP_2 MOF by Yaghi and co-workers,[123] demonstrated the presence of an analogous extended layer trapped in an alternating stacking pattern with the interpolated layer comprising of metal-capped hexahydroxytriphenylenes, leading to an ABAB stacking pattern (**Figure 4A, bottom**).

Ni^{II} salt coordinating to hexaaminotriphenylene (HITP) affords 2D layers arranged in slipped parallel planes within an AAAA stacking pattern (**Figure 4B**).[70, 122] This was shown by Dincă and co-workers through structure simulation and analysis with powder X-ray diffraction. Aspuru-Guzik provided key computational analysis on the stacking mode of Ni_3HITP_2 with the contour map of the potential energy surface leading to further evidence for slipped parallel stacking.[122] When the crosslinking heteroatom on the triphenylene core is interchanged to sulphur (HTTP), two new stacking modes can present themselves (**Figure 4C**). Eclipsed stacking mode is observed with Co^{II}, Ni^{II}, and Cu^{II} metal salts used as a building block for MOF synthesis. Interestingly, when the metal salt is changed to Pt^{II}, the stacking changes to a staggered mode.[140]

Despite synthetic accessibility of layered conductive MOFs, further progress is needed to control the morphology of the crystallites. To date, only one single crystal structure of a 2D MOF has been reported to yield precise structural information and single crystal conductivity measurements.[123] The current knowledge of this class of materials is largely based on studies of bulk materials or thin films comprising microcrystalites with minimal control over their orientation. While accessible morphologies of crystallites include both nanorods[68, 123] or nanosheets,[138, 142] the control over crystallographic morphology and epitaxial orientation is currently limited to using synthetic strategies that involve layer-by-layer assembly.[143]

Overall there has been remarkable progress in the field of 2D conducting MOFs with applications spanning chemical sensing, field-effect transistors, energy conversion, energy storage, and catalysis (**Table 1**). With greater understanding and control over the structure-property relationship, 2D conducting MOFs have the potential to make a lasting impact as broadly applicable multifunctional materials.

Table 1. List of electrically conducting 2D MOFs with the ligand, metal, MOF name, and application.

MOF	Electrical Conductivity	Application	Performance	Ref
Cu_3HHTP_2 [a]	2×10^{-3} S/cm [f]	chemiresistors	alcohols, aliphatics, amines, aromatics, ketones, ethers, study at 200 ppm	144
Cu_3HITP_2 [a]	2×10^{-1} S/cm [f]			
Ni_3HITP_2 [a]	2 S/cm [f]			
Cu_3HITP_2 [a]	2×10^{-1} S/cm [f]	chemiresistors	NH_3 - LOD 0.5 ppm; range of study 0.5 -10 ppm	67
Cu_3HHTP_2 [b]	0.02 S/cm [g,k]	chemiresistors	NH_3 - LOD 0.5 ppm; range of study 1-100 ppm	143
Ni_3HHTP_2 [a]	2.8 ± 0.5 MΩ/cm^2 [i]	chemiresistors	Range of study 5-80 ppm, H_2S - LOD 0.23 ppm, NO - LOD 1.4 ppm	131
Ni_3HITP_2 [a]	5.6 ± 2 MΩ/cm^2 [i]		H_2S- LOD 0.52 ppm, NO - LOD 0.16	
Fe_3HHTP_2/graphite[a]	3.2×10^{-2} S/cm [h]	chemiresistors	Range of study 5-80 ppm, array - H_2S - LOD 35 ppm, array - NH_3 - LOD 19 ppm, array - NO - LOD 17 ppm	130
Co_3HHTP_2/graphite[a]	9.8×10^{-1} S/cm [h]			
Ni_3HHTP_2/graphite[a]	3.8×10^{-2} S/cm [h]			
Cu_3HHTP_2/graphite[a]	2.8×10^{-1} S/cm [h]			
Cu_3HHTP_2 [a]	$7.6 \times 10^{-3} \pm 0.3 \times 10^{-3}$ S/cm [h]	chemiresistors	Range of study 2.5-80 ppm, array - H_2S LOD 40 ppm, array - NO LOD 40 ppm	68
Ni_3HHTP_2 [a]	$1.0 \times 10^{-2} \pm 0.3 \times 10^{-2}$ S/cm [h]			
Cu_3HHTP_2 [a]	n/a	electrochemical ion sensing	11.1 μA/h, K^+ - LOD 6.31 ± 0.01 × 10-7 M, NO_3^- - LOD 5.01 ± 0.01 × 10-7 M	145
Ni_3HHTP_2 [a]	n/a			
Co_3HHTP_2 [a]	n/a			
CoBHT	n/a	hydrogen evolution	overpotential, solution H_2SO_4, pH = 1.3, -0.19 V	146
NiBHT	n/a		-0.33 V	
FeBHT	n/a		-0.47 V	
THTNi 2DSP	n/a	hydrogen evolution	overpotential, solution 0.5 M H_2SO_4, -0.33 V	139
	n/a			
	n/a			
$[Co_3(BHT)_2]^{3-}$ [b]	n/a	hydrogen evolution	overpotential, solution H_2SO_4, pH= 1.3, -0.34 V	63
$[Co_3(THT)_2]^{3-}$ [a]	n/a		-0.53 V	
Cu-BHT[b]	280 S/cm [h]	hydrogen evolution	overpotential, solution H_2SO_4, -0.45 V or -0.76 V	147
NiAT [b]	3×10^{-6} S/cm [j,k]	hydrogen evolution	overpotential, solution H_2SO_4, pH =1.3, -0.37 V	148
NiPc-MOF [d]	0.2 S/cm [h]	water oxidation	low onset, <1.48 V, overpotential <0.25V	141
Ni_3HITP_2 [a]	40 S/cm [g]	oxygen reduction	onset 0.82 V, overpotential 0.18 V	149
Ni_3HITP_2 [a]	40 S/cm [g]	supercapacitors	capacitance, 111 F/g, 18 mF/cm^2	65
Cu_3HHTP_2 [a]	3×10^{-1} S/cm [f]	supercapacitors	capacitance, 120 F/g, 22 mF/cm^2	150
Ni_3HAB_2 [c]	n/a	supercapacitors	capacitance, 420 F/g, Ni = 1.6 F cm^{-2} Ni =760 F/cm^3	151
Cu_3HAB_2 [c]	n/a		capacitance, 215 F/g; Cu= 0.86 F cm^{-2}; Cu n/a	
Co_3HTTP_2 [a]	3.4×10^{-9} S/cm [h]	electrochemical capture of ethylene	ethylene captured, 126.8 mmol/g	152
Ni_3HTTP_2 [a]	3.6×10^{-4} S/cm [h]		218.2 mmol/g	
Cu_3HTTP_2 [a]	2.4×10^{-8} S/cm [h]		100.2 mmol/g	
Ni_3HITP_2	40 S/cm [g]	field-effect transistors	48.6 cm^2/Vs, p-type	153
M-HIB [e]	n/a [m]	field-effect transistors	slight variation in conductance with variation of a back-gate voltage	142
Cu-BHT [a]	1×10^3 S/cm [h,n]	field-effect transistors	116 cm^2/Vs	154

[a] Structural analysis of MOF crystallinity confirmed with PXRD. [b] Structural analysis of MOF crystallinity confirmed by PXRD, and SAED. [c] Structural analysis of MOF crystallinity confirmed by PXRD, SAED, and GXID. [d] Structural analysis of MOF crystallinity confirmed by PXRD, XRD, and synchrotron. [e] Structural analysis of MOF crystallinity confirmed by SAED. [f] Conductivity measurement analysis on a compressed pellet using a two-point probe. [g] Conductivity measurement analysis on a film using a two-point probe. [h] Conductivity measurement analysis on a compressed pellet using a four-point probe. [i] Conductivity measurement analysis on a fabric using a two-point probe. [j] Conductivity measurement analysis on a pellet using van der Pauw. [k] Description of conducting pathway is strong charge delocalization between Cu ions and ligands. [l] Description of conducting pathway is strong charge delocalization. [n] Description of conducting pathway is insulating charge transport behaviour. [n] Description of conducting pathway is strong balanced ambipolar charge transport.

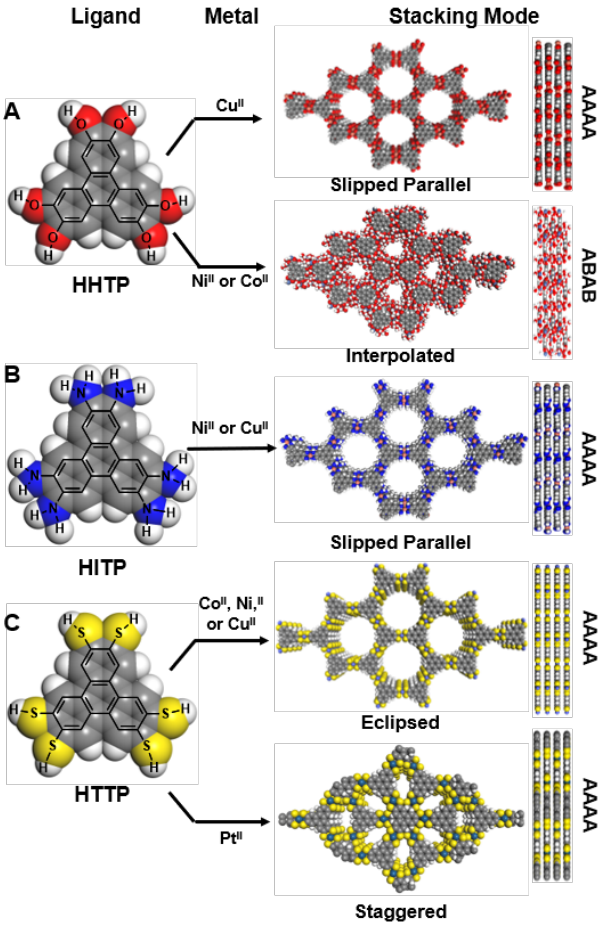

Figure 4. Three triphenylene based organic ligands have been studied with the heteroatom interchanged between O (A)[123], NH (B)[67, 122], and S (C)[125, 139, 140, 152]. The heteroatom present on the triphenylene and the metal salt dictates the formation of MOF and the stacking mode which can vary from slipped parallel, eclipsed, staggered, and with or without the presence of an interpolated layer leading to either AAAA or ABAB pattern.

Methods of Integration of 2D MOFs into Electronic Devices

The multifaceted characteristics of 2D MOFs such as porosity[65], catalytic activity,[63, 149] field-effect,[153] magnetism,[137, 155, 156] and response to chemical stimuli combined with excellent electrical conductivity[124, 125] further reinforce the utility of 2D metal-organic frameworks as new generation of multifunctional materials. Despite the recent advancements in the preparation strategies of 2D conductive MOFs, a critical step towards accessing and optimizing the electronic properties of these materials lies in the robust integration of these materials into functional electronic devices.[58]

This section describes four major integration methods that have been established for the fabrication of functional MOF-based electronic devices. These techniques can be categorized into two types: 1) direct integration, where the MOF is grown onto the pre-selected substrate in a controllable manner using either templated bottom-up self-assembly[68, 130, 131, 152] or liquid-phase epitaxy[143] or 2) stepwise integration involving two distinct steps: MOF synthesis and MOF integration. Each described method offers distinct advantages and limitations including the varying degree of synthetic control of the MOF structure, the overall time required for device fabrication, or the need for additional processing step. Nonetheless, these methods offer capabilities for integrating 2D conductive MOFs into functional devices and thus allow to harness the unique properties of 2D conductive MOF in practical applications.

Drop-casting

Drop-casting is a rapid, straightforward, and a commonly used approach to integrate materials into functional devices.[144] It is a two step-fabrication process in which a synthesized material is initially dispersed in a solvent, and then drop-cast onto the surface of a substrate (**Figure 5A**).[157] This method has been used to produce simple MOF-based chemiresistive sensors capable of sensing toxic gases at sub-ppm levels.[67] Our group utilized drop-casting to generate conformal coatings of MOF layers on customized gold electrodes to achieve electrochemically-driven capture and release of ethylene in a solid-state device.[152] We also used this approach to integrate MOFs into layered device architectures to produce functional potentiometric devices with excellent signal stability and ability to sense biologically and environmentally important ions at sub-micromolar concentrations.[145]

While drop-casting can be straightforward to implement and can be broadly applicable, it does have several limitations. Achieving a dispersion of an insoluble material, such as a typical MOF powder, which requires sonication of the powder in a dispersant (e.g., aqueous or non-aqueous) to create a suspension. This process can induce changes in crystallinity of materials or introduce structural defects. Furthermore, the MOF suspension may be prone to aggregation, and thus exhibit limited stability. While the use of surfactants may help reduce aggregation, the surfactants may introduce undesirable structural changes to the materials and may require removal. Although sonication of the bulk MOF material possesses several limitations in the context of MOF integration into devices, this mechanical force method has been successfully applied to exfoliate bulk 3D and 2D MOFs into layered MOF nanosheets.[1, 53] However, the utility of this approach has not yet been demonstrated in the preparation of nanolayer 2D conductive MOFs. We envision that further advancements in the development of top-down exfoliation strategies may give rise to ultra-thin 2D nanomaterials with unique electronic properties and enhanced surface-to-volume ratio, which are beneficial for applications in electronics and gas storage.[2, 53, 158-161] The non-homogeneity in the drop-casted layer can cause irregularities in solvent evaporation, introducing undesirable non-uniformity in MOF film thickness. Drop-cast layer may also exhibit limited mechanical stability due to poor adhesion between the material and the substrate. The limitations can be minimized through strategic process development and may be acceptable for proof-of-concept studies of randomly-oriented thin films of MOFs crystallites within devices. However, precise examination of structure-property relationships of MOFs within electronic devices would be benefit from development of device

integration methods that offer control over the distribution, thickness, and epitaxial orientation of MOFs in devices.

Mechanical compression and abrasion

Mechanical compression involves the compression of the powdered material, using a mold, into the desired architecture.[65, 130, 144] The compressed powders can be probed directly or abraded onto substrates to facilitate the deposition of a thin film into a device (**Figure 5B**). This integration method can offer an attractive alternative to solution-phase techniques in cases where i) the investigated material exhibits limited chemical or mechanical stability to solvents; ii) the compressed solid possesses coordination properties towards solvent molecules that can diminish its functional performance; iii) the presence of solvents may damage the device architecture or cause irreversible changes to the underlying substrate; and iv) the entrapment of solvent in the pores of the material may be difficult to remove and may have a detrimental effect of device performance.

Dincă et al. utilized mechanical abrasion to fabricate a cross-reactive sensor array that could reliably distinguish between different categories of volatile organic compounds in the chemiresistor configuration.[144] Our group has extended the utility of this method by drawing chemiresistive sensor arrays from four MOFs/graphite blends for detecting and differentiating NH_3, H_2S, and NO at parts-per-million concentrations.[130] Mechanical compression has also been successfully applied for the integrations of MOFs for energy-storage applications.[65, 151]

Even though solvent-free methods are compatible with a broad range of device architectures, they also have several inherent limitations. The high degree of mechanical force applied to construct a packed solid may induce defects in the structure of the MOF and permanently diminish its crystallinity and porosity. Such defects may alter or diminish the performance of fabricated devices, especially if high degree of porosity is required as for gas[152] or energy storage applications.[65] Despite the limitations, this method is well-suited for rapid prototyping of MOF-based technologies with customizable (size and shape) device architectures.

Templated bottom-up self-assembly

Templated bottom-up self-assembly (direct growth) allows direct integration of the material onto targeted substrates without any additional processing steps (**Figure 5C**).[68, 131] While this preparatory method of 2D conductive MOFs is relatively new, it is well established in the synthesis of non-conductive MOFs.[162, 163] As the direct growth method relies on the self-assembly of atoms and molecules into thermodynamically stable crystalline structures, the resulting material can be designed to exhibit high hierarchical order and porosity, advantageous to optimizing performance of fabricated devices.[164]

Direct growth is particularly attractive for one-step rapid fabrication of functional MOF based electronics. Our group demonstrated the utility of this method by growing MOFs on fabrics to generate conformally-coated flexible electronic textiles with high porosity and multifunctional ability to sense, capture, and filter toxic gases.[131] We have also shown the ability to grow randomly oriented mats of MOF-based nanowires on polymeric substrates equipped with graphite electrodes to produce extended conductive surfaces in chemiresistive devices.[68] This assembly method has also been applied to fabricate energy storage devices,[165] and electrocatalysts for energy conversion.[166]

Although this experimental approach enables direct integration, it also has several distinct features that are required for optimal implementation: 1) favourable points for MOF nucleation sites that can facilitate good adhesion of MOF to substrate in solution, 2) compatibility of the substrate with the conditions that may be required for MOF synthesis, such as elevated temperatures, presence of organic solvents, or potentially corrosive substances. Thus, while extremely attractive for certain applications, this method may be somewhat limited in scope, and best suited for MOFs/substrate combinations that can ensure good adhesion in solution and that can be synthesized under relatively mild conditions.

Liquid-phase epitaxy/layer-by-layer growth

Liquid-phase epitaxy can be used to create stable and homogenous coatings of MOF layers, with controlled thickness and orientation, on a solid substrate, providing a promising model for studying the structure-property relationship in MOF materials.[167] This interfacing method refers to the deposition of a MOF on the well-defined surface of a crystalline substrate, with the over-layer having the same crystalline orientation as the substrate,[168] and while it has been already widely employed for the fabrication of non-conductive MOFs,[169, 170] it has only recently been applied to making 2D conductive MOF films. Yao et al. functionalized the surface of sapphire, glass, Si/SiO_2 and quartz substrates through chemical treatments to imbed chemical anchors such as -COOH or -OH that mimic the ligands used in normal solvothermal synthesis.[143] This specifically modified surface acted as a template for MOF deposition/growth resulting in a highly oriented MOF films with well-controlled thickness for practical utility in chemiresistive sensing of ammonia (**Figure 5D**).[143]

Although epitaxial growth method allows the precise control over the MOF deposition onto the solid substrate, and has demonstrated attractive performance, it also has disadvantages: 1) the deposition/fabrication process requires to be individually tailored for the chosen substrate and a MOF.[168] 2) The need for sequential deposition steps may result in lengthy and repetitive sequences that require automation for practical implementation.[171] These limitations may be overcome by advances in surface-coordination chemistry and high-throughput automation. Owing to the well-defined chemical compositions and structural feature of epitaxially grown films, this interfacing method is an excellent choice for fundamental investigations of structure-property relationships in MOFs.

In summary, several distinct methods have been developed for the integration of 2D conductive MOFs in electronic devices. These methods vary in their precision and control and so far, the most precise options available require layer-by-layer assembly.[143] A number of methods have been implemented to put MOFs into a diverse set of substrates such as drop-casting[144, 145] or mechanical compression/abrasion[130, 144] but with limited epitaxial control and morphology of the crystallites, with the exception of layer-by-layer assembly.[143] Although methods of integration are currently limited for 2D MOFs, many opportunities exist for drawing methods from 3D MOFs and 2D nanomaterials which include ink-jet printing and chemical vapor deposition, respectively ultimately leading towards control over structure and morphology of the 2D MOFs in devices.

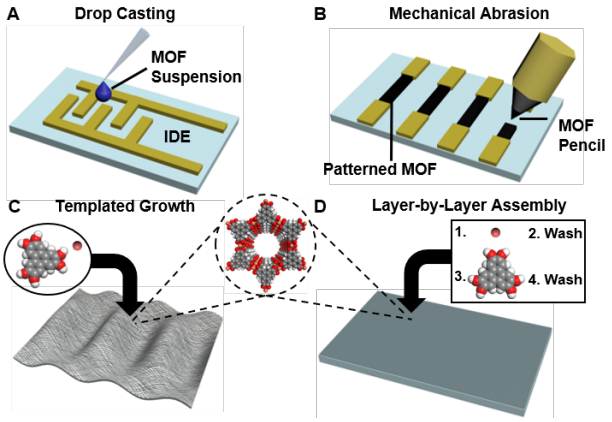

Figure 5. General methods of integrating 2D conductive MOFs into devices. A) In drop casting, bulk MOF is suspended in a solvent and subsequently dropped onto the substrate of interest apply a coating of MOF.[144, 145] B) Mechanical abrasion involves the compression of bulk MOF powder a pellet in the form of a pencil to draw MOF patterns on select substrates.[130, 144] C) Templated growth synthesizes MOFs directly on the substrate of interest and forms effective and conformal contact.[68, 131] D) Layer-by-layer assembly carefully controls the growth of MOFs by exposing the substrate to a solution of metal node and organic linker sequentially.[143]

Applications

To date, the family of 2D conductive MOFs, made of extended hexatopic organic ligands, has received considerable attention as advanced electroactive functional materials due to their unique physical, chemical and electrical properties. We, thus, identified at least three advantages for their multifaced utility in in electronics. *First,* a large degree of structural control and compositional modularity can be achieved through bottom-up synthetic approaches, permitting the integration of known electrocatalyst into the MOF framework (e.g., metallic nodes).[172] *Second, 2D MOFs* exhibits good conductivity making them well-suited for electrically transduced sensing and catalysis.[70, 122] *Third,* the high porosity and surface area presents numerous available active sites necessary for energy conversion and energy storage.[65] We believe that these characteristics offer the possibility to develop conductive MOFs into versatile and integral components of electrochemical technologies.

Electrically-transduced chemical sensing

2D conductive MOFs possess at least six attractive features for broad applicability in electronically-transduced chemical sensing. *First*, as a subclass of all MOFs, 2D conductive MOFs are easily accessible through bottom-up solution-phase synthesis. This ease of access can enable rapid development and optimization of methods for MOF preparation that are not restricted to highly specialized procedures and expensive equipment that are often necessary for the preparation of other 2D nanomaterials using bottom-up fabrication techniques. In principle, any standard chemical laboratory—including high school and college laboratories[173, 174]— can accommodate and train students to execute certain versions of MOF synthesis, with general skills and techniques transferrable to the preparation of layered 2D MOFs. *Second*, 2D conductive MOFs possess conductivity for electronic transduction that is broadly comparable to that of conductive polymers and 2D nanomaterials, making these MOFs excellent candidates for integration into electronic sensing architectures.[1, 70, 78, 172, 175] *Third*, low-dimensionality and high surface-to-volume ratio of individual or few-layers of MOFs are advantageous for maximizing sensitivity in chemical sensing. *Fourth*, the intrinsic porosity of MOFs can facilitate analyte uptake into the material and provide unique modes of interaction with the material's surface that are not available in non-porous 2D materials. *Fifth*, the structural modularity of MOFs achievable from synthetically-tuneable molecular building blocks can enable highly tailored integration of host-guest interactions imbedded within the scaffold. And *finally*, the multifunctionality of 2D conductive MOFs—such as the combination of electrical transport and modular surface chemistry—make them excellent candidates for exploring and harnessing the synergistic effects of molecular design strategies coupled with charge transport.

The first implementation of a 2D layered MOF in electronically-transduced chemical sensing was demonstrated by Dincă and co-workers by integrating Cu_3HITP_2 MOF within a chemiresistive sensing device. Drop-casting of Cu_3HITP_2 onto interdigitated gold electrodes,[67] produced devices capable of detecting NH_3 gas at sub-ppm detection limits (0.5 ppm) at applied potential of 100 mV at room temperature. Sensing performance was unaltered in the presence of humidity (< 60%). Interestingly, the isostructural Ni_3HITP_2 MOF did not exhibit chemiresistive response towards NH_3, thus demonstrating that the selectivity of chemiresistive MOF-based devices can be potentially controlled by the choice of metallic nodes.

Extending the applicability of MOFs in chemiresistive detection, Dincă and co-workers have subsequently developed a cross-reactive sensing array comprising of Cu_3HHTP_2, Cu_3HITP_2, and Ni_3HITP_2 MOFs integrated into a chemiresistive devices either through drop-casting by mechanical abrasion using a compressed MOF powder (**Figure 6A**).[144] Linear discriminate analysis (LDA) and principle component analysis (PCA) enabled differentiation of several classes of volatile organic compounds (VOC) with 90% accuracy at 200 ppm. VOCs

included alcohols, aromatics, ketones/ethers, amines, and aliphatics.

While the specific mechanism of binding was not elucidated, the authors indicated that multiple competitive binding mechanisms are simultaneously operating in the studied MOFs including charge transfer mechanism or hydrogen bonding.[144]

A significant enhancement in chemiresistive sensing using layered 2D MOFs was recently developed by Yao et al. using epitaxially-oriented thin-films of Cu_3HHTP_2 MOF prepared through layer-by-layer liquid-phase epitaxial method (**Figure 6B**).[143] The thin-layer formation was made possible by the use of pre-functionalized substrates in which the hydroxyl groups (-OH) created a template for the oriented film growth. The resulting devices exhibited low-ppm sensitivity to ammonia (LOD of 0.5 ppm) and only limited response to 10 other gases and vapours including benzene, CO, ethanol, ethylbenzene, H_2 methane, methanol, n-hexane, and toluene, highlighting potential for good selectivity. Interestingly, the response and recovery time was up to 54% faster than observed for bulk powder counterparts. This observation was attributed to enhanced contact of gaseous analytes with the active sites in the MOF with minimal diffusion barriers.[143]

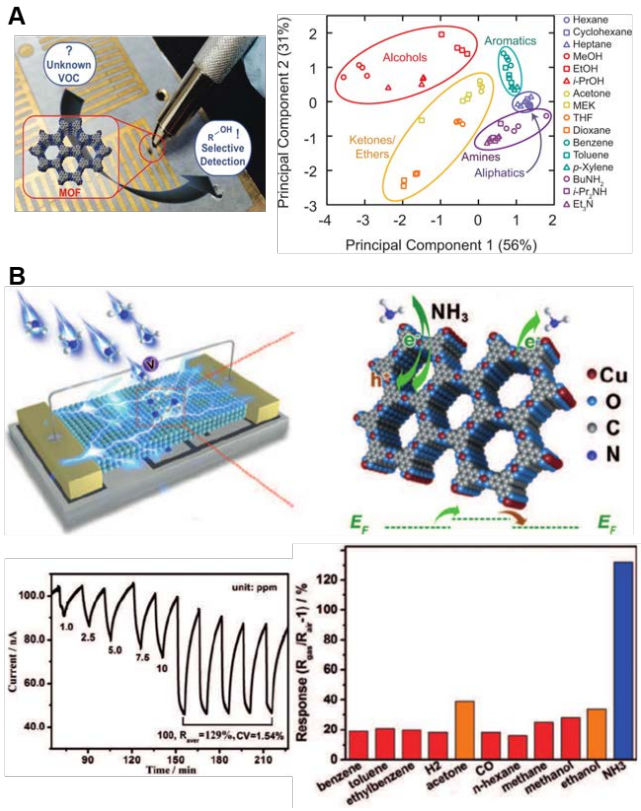

Figure 6. A) Fabrication of MOF-based chemiresistors by "drawing" onto gold electrodes on paper, using a compressed pellet of MOF. Principal component analysis of MOF senor array's response to volatile organic compounds.[144] B) Room temperature gas-sensing performances of Cu_3HHTP_2. The gas sensor and possible gas-sensing mechanism. The response–recovery curve toward NH_3 with different concentrations. The column chart of responses toward different reducing gases of Cu_3HHTP_2-10C.[143]

Broadening the implementation of MOFs in chemiresistive sensing, our group has focused on the development of direct integration techniques that do not rely on drop-casting or mechanical abrasion to create several unique device architectures. Our first demonstration of using direct assembly for integrating 2D conductive MOFs into a chemiresistive device featured the installation of 2D conductive M_3HHTP_2 MOFs (M = Ni and Cu) into polymeric device chips equipped with pre-patterned graphitic electrodes.[68] The method generated mats (15 μm in thickness) of randomly-oriented MOF nanowires. The resulting miniaturized devices Cu_3HHTP_2 and Ni_3HHTP_2 successfully differentiated between gas-phase NH_3, NO, and H_2S at ppm concentrations (10-80 ppm).[68]

Extending the generality of direct assembly of MOFs into devices, we fabricated multifunctional electrically conductive textiles through direct solution-phase growth of Ni_3HHTP_2 and Ni_3HITP_2 MOFs from their molecular precursors on flexible fabric-based substrates (**Figure 7A**).[131] The resulting Self-Organized Frameworks on Textiles (SOFT) exhibited good mechanical stability and uniquely capitalized on the porosity of both constituent components: the MOF and the fabric. SOFT sensors were simultaneously capable of detecting, capturing, and filtering NO and H_2S with sub-ppm limits of detection (NO = 0.16 ppm and for H_2S = 0.23 ppm) and uptake capacity of 12-23 mmol of gas per mg of MOF. The chemiresistive response was largely unaffected by the presence of humidity (18% RH) and was fully recoverable by washing the SOFT sensors in water. This behaviour implied the potential reversibility of MOF-analyte interactions in aqueous environments.[131]

To broaden the applicability of solvent-free methods for integrating MOFs into devices, our group has also developed a rapid-prototyping approach for fabricating chemiresistive sensing arrays based on M_3HHTP_2 MOFs/graphite blends (M = Fe, Co, Cu, Ni).[130] The formation of graphite/MOF blends was necessary to establish electrical contact within sensing devices and allow direct integration of only moderately conductive MOFs that alone presented challenges with producing a continuous charge transport pathway within simple electrically transduced sensors. This method produced devices capable of detection and differentiation of NH_3, NO, and H_2S at ppm-concentrations.[130]

To expand and demonstrate the broad potential utility of MOFs in electroanalysis beyond amperometric chemiresistive devices, our group has recently illustrated the applicability of 2D conductive MOFs (Ni_3HHTP_2, Cu_3HHTP_2, and Co_3HHTP_2) as ion-to-electron transducers in potentiometric sensing of ions (**Figure 7B**).[145] We fabricated multilayer potentiometric sensing devices for K^+ and NO_3^- ion detection using M_3HHTP_2 MOFs (M = Cu, Ni, and Co) by drop-casting the MOFs on top of glassy carbon electrodes, and covering them with a layer of polymeric ion-selective membranes. Fabricated devices exhibited excellent signal stability of 14.6 μV/sec under polarizing conditions (1 nA), low long-term drift (11.1 μV/sec), and high sensitivity to K^+ and NO_3^- of $6.31 \pm 0.01 \times 10^{-7}$ M and $5.01 \pm 0.01 \times 10^{-7}$ M, respectively. These observations were ascribed to large double-layer

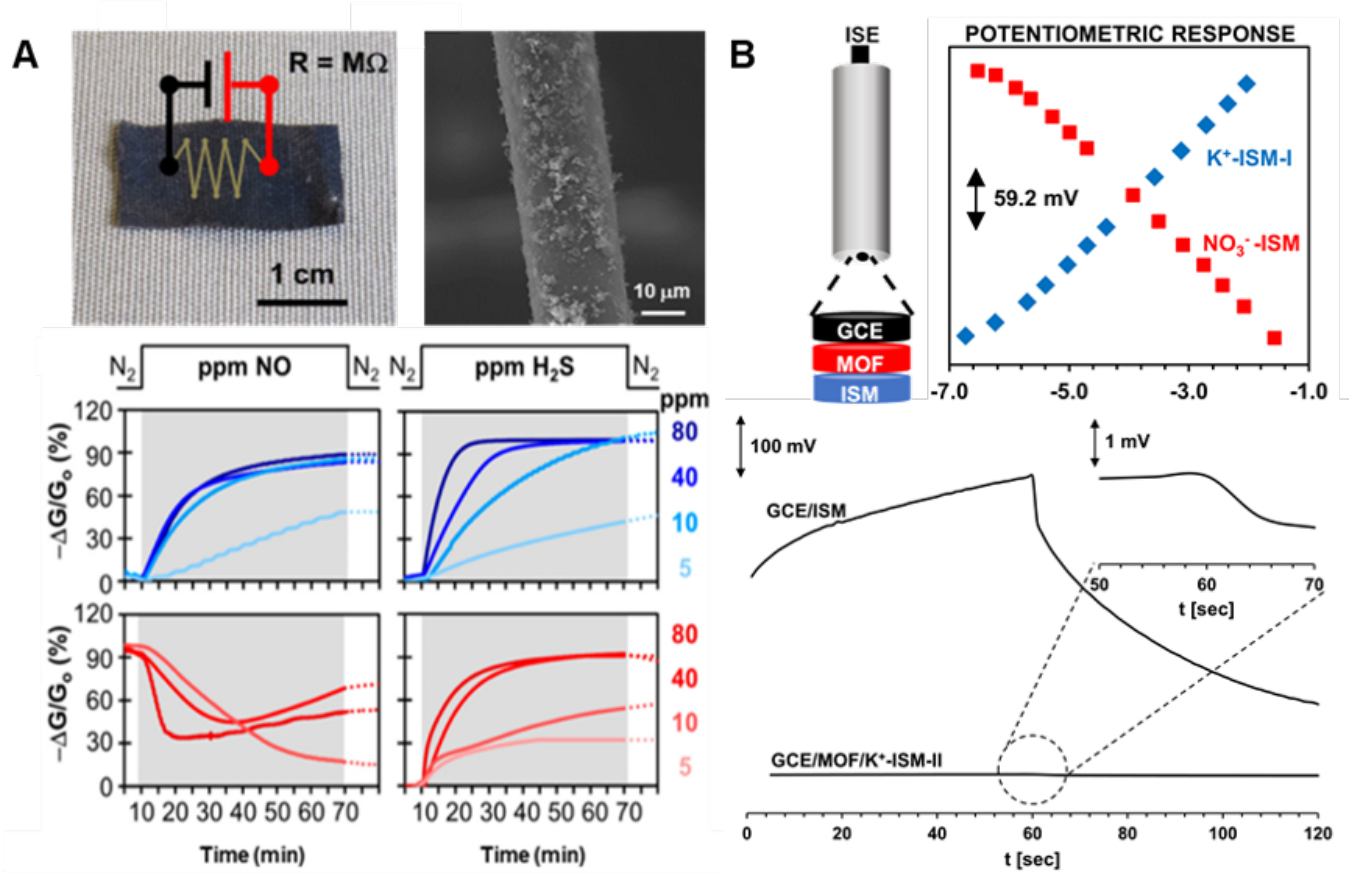

Figure 7. A) Photograph of cotton SOFT-sensor: textiles coated with nanoporous MOF. Scanning electron microscope image of self-assembled MOF grown on the individual fibres of the textile. Representative response for Ni_3HITP_2 (blue) and Ni_3HHTP_2 (red) SOFT-sensors when exposed to (from left to right) NO or H_2S. Slope (m) of first 5 min of sensor response versus concentration of analyte, in response to NO (left) and H_2S (right).[131] B) Schematic representation of layered electrode architecture used for potentiometric measurements.[145] In this configuration, a thin film of 2D MOF was drop-casted directly on the top of a glassy carbon electrode (GCE), and then covered with an ion-selective membrane (ISM) to enable potentiometric ion sensing. Potentiometric response of GCE/Ni_3HHTP_2 MOF/ISM devices to K^+ (red squares) and NO_3^- (blue diamonds) ions. Chronopotentiograms obtained during the analysis of K^+-ISM-II based ISEs under polarizing conditions. (Top) K^+-ISM-II applied directly onto a GCE contact without the MOF as undelaying conductive layer; (Bottom) GCE/Ni_3HHTP_2 MOF/K^+-ISM-II electrode. Inset demonstrates a close-up of response obtained for the GCE/Ni_3HHTP_2 MOF/K^+-ISM-II. Experimental conditions: applied current +1 nA for 60 seconds followed by -1 nA for 60 seconds in 0.1 M KCl.[145]

capacitance (204.1 µF) in MOF-coated electrodes. The ion-to-electron transduction was hypothesized to proceed through the formation of electrical double layer in the case of Ni_3HHTP_2 and Co_3HHTP_2 MOFs and with an additional contribution from redox doping/undoping in Cu_3HHTP_2 MOFs.[145]

2D MOFs have been developed as active materials in chemiresistive and potentiometric sensors. Despite this progress, host-guest interaction between MOFs and analytes are not well established. While several hypotheses have been drawn, the is still lack of conclusive evidence for characterizing the sensing mechanisms.[130, 143, 144] The fundamental insight into host-guest interactions is a crucial aspect that needs further investigation to ensure rational molecular design of 2D MOFs for chemical sensing.

MOF-based electronics

Field-effects modulate the electric and magnetic field to influence the behaviour of the device leading to fundamental understanding in charge carrier mobility, charge carrier type, and carrier concentration, ultimately leading to new and improved electronic applications.[153] 2D MOFs possess attractive features that make them applicable to electronic devices, such as low-dimensionality for compact device implementation,[96, 99] structurally tuneable bandgap,[176] and possibility for unique magnetic exchange interactions.[137, 155]

In 2017, Louie and co-workers demonstrated the controlled growth of M_3HAB_2 (M=Co, Ni, and Cu) thin films that were subsequently integrated into FET devices using a lift-off technique.[142] Laterally large (µm) but also ultrathin MOF films were synthesized through a biphasic method. The interfacial synthesis was conducted with the metal salt dissolved in an aqueous layer and the organic linker dissolved in the EtOAc layer then the MOF forms at the liquid/liquid interface. Ni_3HAB_2 showed a gate-dependent conductance down to 4 K. The devices generally decreased in conductance with lower temperature, indicating semiconducting behaviour.[142]

While Louie and co-workers used the liquid/liquid interface, Xu and co-workers examined the application of a versatile liquid-air synthetic approach to fabricate ultrathin (<50 nm) films of Ni_3HITP_2 MOF (**Figure 8A**).[153] The porous FET demonstrated p-type behaviour with great charge mobility with 48.6 $cm^2\ V^{-1}\ s^{-1}$at room temperature. MOF films were initially

transferred onto the FET devices using the Langmuir-Schaefer transfer method. The conductivity of Ni_3HITP_2 followed an exponential decrease upon cooling, revealing the semiconducting nature of the MOF. Based on the temperature dependent conductance, the authors proposed at least two types of conduction mechanisms: thermal activation at higher temperatures (>240 K) and hopping conduction at lower temperatures (< 240 K).[153]

The group of Marinescu tested the temperature depended conductance of Co_3HTTP_2 (**Figure 8B**).[125] At 300 K the bulk conductivity of a pressed pellet of Co_3HTTP_2 was measured to be 1.4×10^{-3} S cm^{-1}. As expected in semiconducting materials with thermally populated carriers, the decrease in temperature (300 to 170 K) led to a decrease in conductivity. Interestingly, between 130 to 50 K the conductivity increased suggesting a transition from the semiconducting to metallic behaviour. The temperature dependent resistivity showed multiple maxima, which the authors attributed to the contributions from stacking faults, local molecular vibrations, and pore-entrapped solvent molecules subsequently producing a complex mechanism for scattering of charge carriers.[125]

Dou et al. reported on the synthesis of crystalline Ni_3HIB_2 and Cu_3HIB_2 MOF which produced pellet conductivities exceeding 800 S cm^{-1} (**Figure 8C**).[124] DFT calculations revealed metallic character in both MOFs with metallic character in the ab direction and semiconducting character in the c direction of the Brillion zone. Ni_3HIB_2 and Cu_3HIB_2 revealed a positive correlation in temperature dependence conductivity.[124]

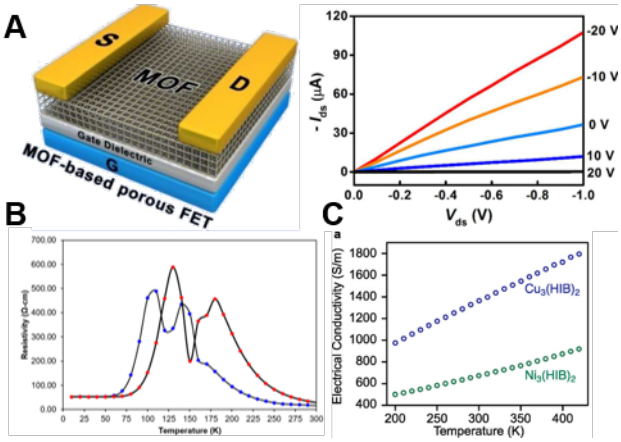

Figure 8. A) Fabrication of MOF-based porous FETs. Electrical characteristics of $Ni_3(HITP)_2$ -based FETs output curves.[68, 153] B) Variable-temperature resistivity data for films of Co_3HTTP_2 with thicknesses of 0.5 µm before (blue) and after (red) 2 h under vacuum at 90 °C.[125] C) Variable-temperature electrical conductivity of pressed pellets of $M_3(HIB)_2$ measured by the van der Pauw method under vacuum.[124]

The fundamental investigation for charge carrier type and development of metallic behaviour in 2D MOFs shows great promise for potential electronic applications.[133, 134, 176] Unlike other 2D nanomaterials, the inherent porosity in 2D MOFs may greatly extend FET based applications which require large surface area and penetrability for the targeted analytes.[153] The exertion of control on the formation of 2D MOFs greatly affects the conductivity of the materials which was demonstrated with the same MOF either possessing metallic conductivity or semiconducting behaviour which is not found in other 2D nanomaterials.

Energy conversion: H_2/O_2 Evolution

The electrochemical splitting of water is one of the most appealing strategies for storing clean and renewable energy in chemical bonds with a possibility of highly efficient conversion into water, electricity, and heat when used in fuel cells.[177] High-performing electrocatalysts for hydrogen evolution reaction (HER), oxygen reduction reaction (ORR), and oxygen evolution reaction (OER) are thus critical to propel the progress in sustainable energy technologies. The HER, ORR, and OER proceed through:[178]

HER: $2H^+ + 2e^- \rightarrow H_2$
ORR: $2H^+ + 1/2O_2 + 2e^- \rightarrow H_2O$
OER: $H_2O \rightarrow 2H^+ + 1/2O_2 + 2e^-$

Despite a handful of superbly performing commercial electrocatalysts, their high cost and poor electrochemical stability have consistently limited their long-term practicality.[179] Thus, inexpensive and scalable electrocatalysts that can facilitate catalytic transformations in HER, ORR and OER with high efficiencies and low energy input must be developed. 2D conductive MOFs are promising substitutes that have been explored to develop advanced electroactive materials for energy transformations. *Firstly,* the large degree of structural tunability of MOFs allows integration of well-defined catalytic units, with known low overpotentials for energy conversion technologies,[63, 146, 178] into the framework of the MOF. *Second,* the permanent porosity facilitates rapid diffusion throughout the electrocatalyst giving rise to enhanced active sites densities. *Third,* the high electrical conductivity can facilitate charge transport during electrocatalytic transformations resulting in low overpotentials for energy conversion applications. *Fourth,* 2D MOFs may exhibit improved hydrolytic stability over other electrocatalysts such as metal nanoparticles, metal oxides or organo-metallic complexes due to the strong nature of metal-ligand bonds in MOF framework. And *fifth,* external guest molecules such as catalytic nanoparticles can be loaded into the MOF, which act as porous scaffold, thus harnessing the synergistic effect for energy conversion applications of both materials.

The integration of HER electrocatalytic units into MOFs is an effective route to prepare high-performance electrodes. In 2015, Marinescu and co-workers, through solvothermal bottom-up synthesis, integrated cobalt dithioline catalytic sites into the $[Co_3(BHT)_2]^{3+}$ and $[Co_3(THT)_2]^{3+}$ MOFs, directly onto the HOPG plate, to obtain effective catalysts for HERs.[63] The authors observed low overpotential for HERs in acidic environment (pH = 1.3) of 0.34 V and 0.53 V at 10 mA/cm^2 for $[Co_3(BHT)_2]^{3+}$ and $[Co_3(THT)_2]^{3+}$ MOFs, respectively. While direct MOF growth on HOPG yielded good catalytic performance towards HERs, the same electrodes prepared through drop-casting method showed limited mechanical stability, and low current-density. The diminishment in the electrocatalytic performance was

caused by the peeling-off of the material from the electrode surface due to H_2 bubbles generated during prolonged electrolysis. The proposed mechanism of HERs in both MOFs involved redox reactions of metal centres (Co^{3+} to Co^{2+}) followed by the protonation of the sulphur sites in the organic ligand.[63]

Dong et al. used the Langmuir–Blodgett method to construct a free-standing single-layer sheet of Ni_3HTTP_2 MOF (0.7–0.9 nm in thickness).[139] Device integration involved transferring the MOF thin-film from the solution interface and placing it directly onto the glassy carbon electrode. This electrocatalyst generated hydrogen gas from 0.5 M sulphuric acid solution at the overpotential of 0.33 V (10 mA cm^{-2}). Good catalytic performance of Ni_3HTTP_2 MOF sheets for hydrogen generation was attributed to their large available surface area which allowed for sufficient exposure of electrocatalytic active sites during the HER.[139] The authors also suggested that HER proceeds through the protonation of S heteroatoms in the bis(dithiolene) as previously reported by Marinescu.[63]

Considerable efforts have been devoted to designing novel MOFs that could serve as electrocatalyst in HERs. In the recent work, Nishihara and co-workers synthesized single layer sheets (0.6 nm) of NiAT that can undergo a reversible interconversion between NiAT and bis(iminothiolato)nickel (NiIT) nanosheet forms through $2H^+ \rightarrow 2e^-$ reaction for HERs.[148] This process was accompanied by large change in conductivity - from 3 x 10^{-6} to 1 x 10^{-1} S cm^{-1} with ferrocenium tetrafluoroborate used as oxidizing agent. The NiAT MOFs drop-cast on GCE covered with a thin layer of Nafion at pH = 1.3 showed the onset potential for HER at -0.15 V (-0.37 V at 10 mA cm^{-2}) and a Tafel slope of 128 mV dec^{-1}. Tafel slope analysis demonstrated that charge transfer was a rate defining step in HERs and demonstrated quick electron transfer kinetics of the catalyst for hydrogen generation. The same electrocatalyst also demonstrated good electrochemical stability for prolonged cycling in acidic conditions (over 500 cycles). The authors calculated that 0.1 s^{-1} molecules of H_2 gas are generated during the HERs using NiAT MOFs at 300 mV overpotential, outperforming other 2D intrinsically conductive MOFs as electrocatalysts in HERs.[148]

Further work by Huang et al. examined the influence of different morphologies of CuBHT (thin film (TF-1), nanocrystals (NC-1) and amorphous nanoparticles (NP-1) on the electrocatalytic performance to HERs in acidic environment (H_2SO_4, pH = 0.0).[147] To aid this investigation, the authors integrated the electroactive materials onto the glassy carbon electrode through drop-casting MOF/Nafion solution. They observed that the overpotential for HER was reduced from 760 mV to 450 mV at 10 mAcm^{-2} when the morphology of the MOF was changed from NC-1 to NP-1, respectively. This remarkable decrease in activation energy for HER was attributed to the Cu-edge site effect on the (100) plane present in the NP-1 of CuBHC and higher interfacial contact area of NP-1 with the background electrolyte if compared to TF-1 or NC-1. Moreover, the authors reported that NP-1 CuBHC electrocatalyst retains approximately 99% of its function in HERs beyond 20 h of continuous operation in a highly acid medium, demonstrating excellent electrochemical stability.[147]

Recently, Downes et al. assessed the influence of coordinated metal (Co, Ni and Fe) on HERs in benzenehexathiolate (BHT) coordination frameworks (**Figure 9A**).[146] The drop-cast layer of MOF on glassy carbon electrode exhibited overpotential for HER in acidic environment (pH = 1.3) as low as 473 mV, 331 mV and 340 mV for FeBHT, NiBHT and CoBHT, respectively. The enhanced activity of CoBHT was attributed to a higher electrochemically accessible surface area and lower charge transfer resistance at smaller overpotentials compared to NiBHT and FeBHT. The authors observed strong thickness dependence on the MOF activity to catalyse HERs. They reported on optimum 244 nm film thickness in which proton diffusion and transfer rates, together with the number of electrochemically accessible active sites were optimized to promote high electrocatalytic activity for hydrogen generation. However, with increasing thickness the charge transfer and proton permeation through the thick films were diminished consequently reducing the electrocatalytic activity of MOFs to HERs.[146]

Oxygen reduction reactions convert H_2 into useful energy through the hydrogen oxidation reaction at the cathode of fuel cells. Miner et al. reported on the first use of 2D conductive MOF (Ni_3HITP_2) in the oxygen reduction reaction (ORRs) in alkaline media (**Figure 9B**).[149] The authors solvatochemically grew 120 nm thin films of Ni_3HITP_2 directly onto the GCE and used it for the oxygen reduction reactions. This demonstrated experimental approach is considered as superior in comparison to other integration techniques as it eliminated the need for binders/additives that may block access to the electrocatalytic active sites in the MOF. The reported on 0.18 V overpotential relative to Pt electrode (E_{onset} =1.00 V) for ORRs in 0.10 M KOH solution (pH = 13.0) was comparable in magnitude with many other non-precious metal-based catalysts. The authors proposed that ORRs proceeds through the one-electron pre-equilibrium reaction (formation of the superoxide anion as the rate-limiting step) further evidenced by Tafel slope of 120 mV/dec. Miner et al. also observed that 88% recorded current density was retained after 8h of continuous electrochemical cycling indicating that 2D conductive MOFs could be potentially used in catalysis of ORRs.[149]

The oxygen evolution reaction (OER) is the anodic reaction of water splitting and is a counterpart to HERs.[178] To enable efficient water splitting it is thus important to design novel electrocatalysts with minimal overpotential for OER that enable long-term stability. In the seminal study, Tang and co-workers developed the NiCo bimetal–organic framework nanosheets (NiCo-BDC) with high electrocatalytic efficiency for OERs.[180] The synthesized NiCo-UMOFNs thin films were dispersed in Nafion-containing solution and subsequently drop-cast onto a glassy carbon electrode and copper foam to from functional devices. The authors observed that GCE-coated electrode exhibits low overpotential for OERs – 250 mV at 10 mA cm^{-2}, which can be further lowered to 189 mV by transferring the thin films onto a copper foam electrode in alkaline conditions (1 M KOH). The improvement in the response was attributed to the excellent conductivity and electron transfer ability of the copper substrates in comparison to GCE. Interestingly, control

experiments with monometallic NiBDC and CoBDC MOFs and bulk powder NiCo MOF were used, revealed that much higher overpotentials for OERs are required: 1.46 V, 1.53 V and 1.48 V, respectively. Tang et al. also reported on great electrochemical stability of the catalyst with 99.3% retention of faradic efficiency after 200h of continuous cycling. They provided experimental evidence that OER reactions proceed through the adsorption of

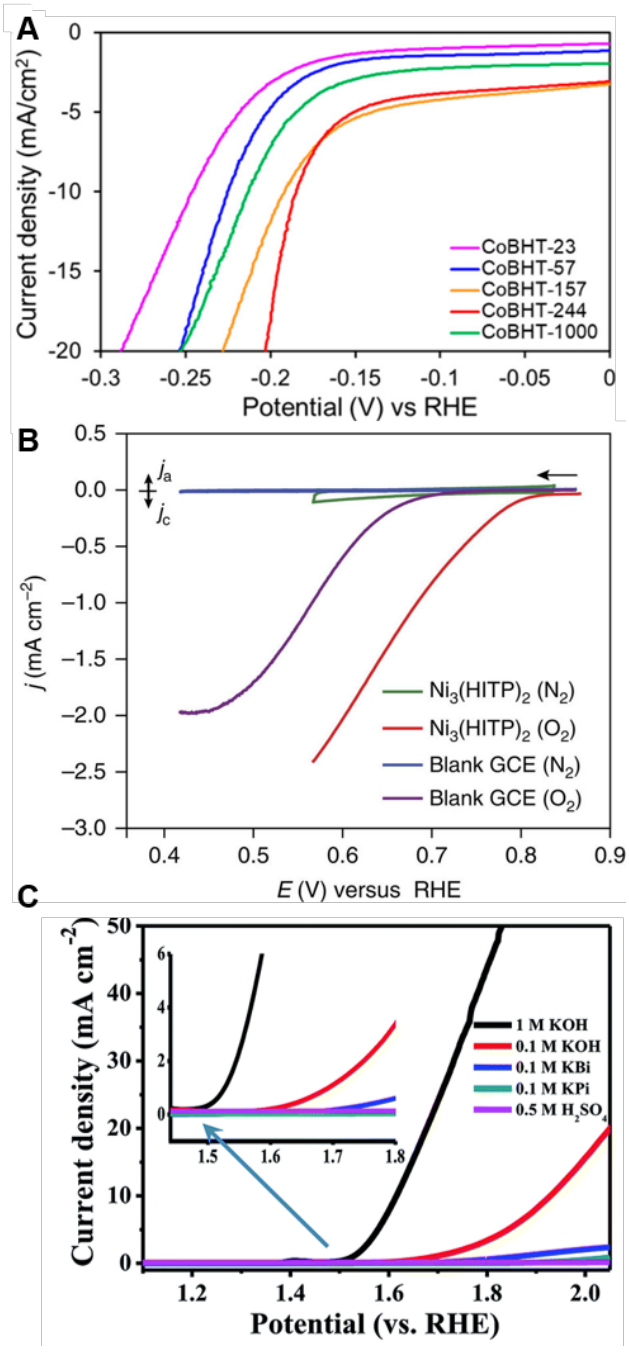

Figure 9. A) Polarization curves for CoBHT-23 (purple), CoBHT-57 (blue), CoBHT-157 (orange), CoBHT-244 (red), and CoBHT-1000 (green); scan rate: 100 mV/s.[146] B) Polarization curves of $Ni_3(HITP)_2$ under N_2 (green) versus O_2 atmosphere (red) as well as of the blank glassy carbon electrode under N_2 versus O_2 atmosphere (blue and purple, respectively). Scan rate=5 mV s^{-1}, rotation rate=2,000 r.p.m., electrolyte=0.10 M aqueous KOH, counter electrode=Pt mesh, reference electrode=Hg/HgO (1.00 M KOH), working electrode=glassy carbon electrode (GCE).[149] C) The pH-dependent LSV curves using the NiPc–MOF as the OER catalyst.[141]

the intermediates onto the unsaturated coordination metal sites (Ni and Co) in the MOF framework. In addition, the authors suggested partial electron transfer from the Ni^{2+} sites to the Co^{3+} sites giving rise to the high activity of the bimetallic MOF for OERs.[180]

Recently, a novel class of 2D conductive nickel phthalocyanine-based (Ni-Pc) MOF was investigated for their catalytic applications in OERs (**Figure 9C**).[141] Jia et al. used bottom-up synthetic approach to integrate Ni-Pc MOFs directly onto the FTO electrodes.[141] The resulting films (100 – 200 nm) yielded satisfactory conductivity (approximately 0.2 S cm^{-1} at RT) and mechanical stability for the use as catalyst in OERs. They observed good electrocatalytic activity for oxygen evolution with estimated overpotential of 0.25 V in 1.0 M KOH and faradic efficiency of 94% after continuous cycling for 6000 seconds. Moreover, Tafel slope analysis (74 mV/dec) confirmed efficient electron transfer kinetics for OERs in Ni-Pc MOFs.[141]

Despite many improvements and large promise in the applications of 2D conductive MOFs as electrocatalyst in energy conversion applications, there are several major challenges that need to be addressed through future research. Chemical stability of many MOFs in aqueous media (acidic, neutral or basic) used in energy transformation reactions can be compromised. In particular, MOF decomposition during electrochemical testing at either strongly reductive or oxidizing applied potentials can be encountered for many MOF based systems.[178, 179] Therefore, strong metal-ligand bonds are required to induce sufficient stability to MOF hydrolysis. For many energy conversion applications, delamination of MOF from the electrode surface over prolonged electrochemical testing is also observed.[178, 179] A more robust and reproducible integration/deposition method needs to be developed to ensure good contact between the material and underlaying electrode especially if such systems were employed in commercial energy applications. And *finally*, the experimental and computational mechanistic investigation of structure-property relationship of 2D conductive MOFs will deepen the understanding of the role of MOF in electrocatalysis and will ideally guide the design of future conductive MOFs for energy applications. Regardless of these challenges, the use of 2D conductive MOFs is an exciting development in the energy conversion field that has not yet converged on a fully satisfactory material solution.

Energy storage

The increasing importance of developing efficient and reliable long- and short-term electrical energy storage devices significantly propelled the development of battery and supercapacitor technologies in the recent years.[181] Depending on the energy-storage mechanism, electrical capacitors can be sub-divided into either electrical double-layer capacitors (EDLC) or pseudo-capacitors.

The capacitance of EDLC systems arises from charge separation at the electrolyte/electrode interface and is thus directly proportional to surface area of material.[182] In contrast,

pseudocapacitive devices store electrical charge via reversible redox reactions. 2D conductive MOFs possess optimal features for their utility as electroactive materials for energy storage applications: they possess high electrical conductivity that is on par or exceeds of other 2D nanomaterials,[122] further leading to increased capacity and rate performance of electrical capacitors. These materials also exhibit high specific surface area necessary for obtaining high capacitance.[65, 151] The modular tunability of the MOF structure also allows for the integration of pseudocapacitive components into the MOF framework that leads to increased density of redox active sites, and consequently enhanced gravimetric and volumetric capacitances. Although, the redox properties of many MOFs are primarily ligand centred, the incorporation of transition metals into the MOF framework (e.g., Fe, Cu, Co) recently allowed to harness their redox activity in energy production and storage applications.[63, 151] Some additional benefits include fully accessible organic molecule–coordinated metal sites and easily tuneable pore structures that can be tailored towards specific electrolyte used for energy storage.

The first example of a supercapacitor made entirely of MOF was shown in 2017 by Sheberla et al. (**Figure 10A**).[65] The authors used Ni_3HITP_2 MOF to fabricate electrochemical double layer capacitor (EDLC) for energy storage applications through compression of MOF powder into a pellet form thus eliminating the need for conductive additives or organic binders.[65] Under these circumstances, the high degree of double layer capacitance exhibited by the Ni_3HITP_2 was mainly dictated by their extremely large surface area and unique porous structure, which allows diffusion of the background electrolyte ions through porous framework. The authors noted high gravimetric capacitance of 111 F g^{-1} at a low discharge rate of 0.05 A g^{-1}.[65] The same EDLC exhibited performance retention over 10,000 cycles and large surface area normalized capacitance of 18 $mFcm^{-2}$. They observed that electrical double layer storage mechanism is dominant in this material with negligible contribution of redox pseudo-capacitance to the recorded response. These performance characteristics are on a par with many EDLCs based on porous carbons, however still does not outperform the optimal materials. The authors identify that further increase in porosity, conductivity and deliberate introduction of redox pseudo-capacitance may give rise to better capacitors.[67]

In the same year, Li et al. used bottom-up synthesis to integrate Cu_3HHTP_2 directly onto the carbon nanowire to form single-material electrode for supercapacitors.[150] They also prepared an analogous Cu_3HHTP_2 MOF electrode through mixing Cu_3HHTP_2 MOF powder with a polymer binder and then coating the material onto carbon paper using slurry-coating method. The proposed Cu_3HHTP_2 MOF nanowire capacitor exhibited capacitance of 120 F g^{-1} at current densities of 0.5 A g^{-1} with specific surface area normalized capacitance estimated at 22 μF cm^{-2}. The authors noted that Cu_3HHTP_2 powder-based electrodes retain approximately 23% of the initial capacitance, at current densities spanning from 0.25 to 5 A g^{-1}, while Cu_3HHTP_2 MOF nanowire can retain up to 55% of the current density probed in the same region.[150] Direct growth of MOF crystals on the carbon fibres provided good mechanical adhesion and consequently reduction of the intrinsic resistance and charge transfer resistance at the electrode/electrolyte interface thus allowing effective charge/electron transport on the MOF nanowire/electrolyte interface. The authors suggested that double layer mechanism is primarily responsible for excellent capacitive response of Cu_3HHTP_2 MOF nanowires as evidenced by the rectangular shaped of the CV.[150]

Different strategy to increase the volumetric and areal capacitance was recently introduced by Bao and co-workers (**Figure 10B**).[151] This research group prepared free-standing electrodes of CuHAB and NiHAB MOFs for energy storage applications by mixing either material with a binder (5% polytetrafluoroethylene (PTFE)) and conductive additive (5% carbon black).[151] During cyclic voltammetry measurements, they observed reversible redox behaviour for both HAB MOFs and large gravimetric capacitances of 420 F g^{-1} for Ni-HAB and 215 F g^{-1} for Cu-HAB. The authors indicated that redox pseudo-capacitance was the primary charge storing mechanism in the studied MOFs with minimal contribution of double layer capacitance (<10 % for NiHAB and <20 % for CuHAB MOFs). Bao and co-workers also prepared compressed pellets of NiHAB MOFs which exhibited exceptionally high volumetric capacitances of 760 F cm^{-3} for a 50 μm thick pellet. Moreover, the MOF electrodes showed good electrochemical stability to continuous cycling with 90% capacitance retention over 12000 cycles. They indicated that the very small particle size of the Ni-HAB aggregates, their substantial porosity that enabled easy access for the diffusion of electrolyte to the active sites, and the intrinsic conductivity of the HAB MOFs were responsible for large volumetric and gravimetric capacitance of studied systems.[151]

The class of 2D conductive MOFs is promising, as an active electrode material, for the development of stable capacitors. However, there are still some challenges with practical implementation of MOFs for energy storage applications. During fabrication of capacitors many of the MOF electrocatalysts either adhere to electrode surfaces through noncovalent interactions, which often leads to surface layer delamination, and consequently a diminishment in performance/stability of a device,[63] or through the compression into the pellet.[65] In particular, mechanical compression may significantly reduce the porosity or even lead to the collapse of porous framework,[152] thus potentially minimizing capacitance of the fabricated device. Additionally, if the deposited films or compressed pellets are not mechanically stable upon contact with an electrolyte, binders such as Nafion are required for electrode construction, which can diminish charge transport and electrocatalytic activity.[178] A more robust approach to integrate the 2D conductive MOFs is thus sought and ideally with future advancements in rapid-prototyping methods such as 3D printing, or ink-jet printing, more stable device architecture could be fabricated. The electrochemical stability of 2D conductive MOFs during operation of capacitors in highly corrosive electrolytes remains another critical issue. Improvements in stability and robustness through strategic

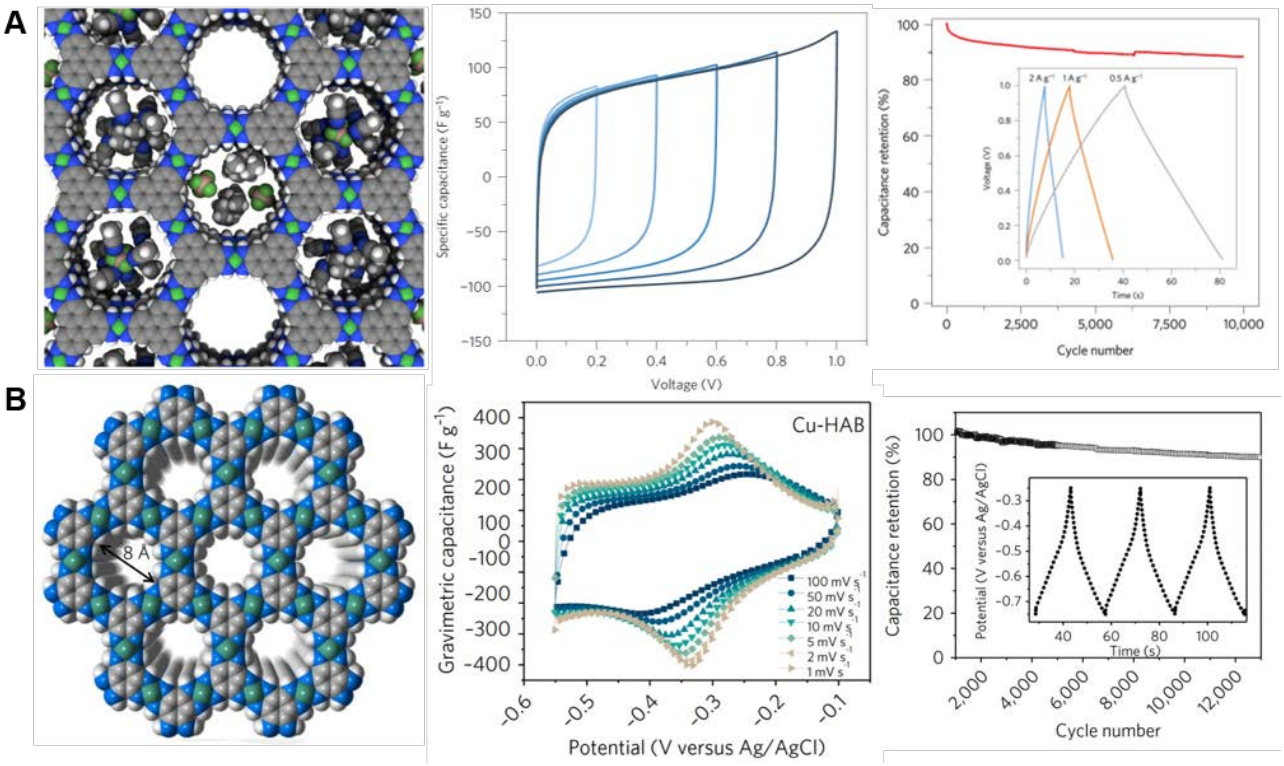

Figure 10. A) Molecular structure of Ni_3HITP_2. Relative size of pores, electrolyte Et_4N^+ and BF_4^- ions, and acetonitrile solvent molecules shown in a space-filling diagram of idealized Ni_3HITP_2. Green, lime, blue, grey, brown, and white spheres represent Ni, F, N, C, B, and H atoms, respectively. Cyclic voltammetry at a scan rate of 10 mV s^{-1} at increasing cell voltage. A slight deviation of the CV trace around 1 V from rectangular shape is attributed to a redox process described in the text. Capacitance retention under repeated cycling at a current density of 2 A g^{-1} for 10,000 cycles. The inset shows galvanostatic charge and discharge curves at current densities of 0.5, 1.0, 2.0 A g^{-1}.[65, 67] B) A space-filling model of the Cu-HAB model. Blue, grey, green and white spheres represent N, C, Ni and H atoms, respectively. Cyclic voltammetry profiles collected at different scan rates for Cu-HAB Capacitance retention data collected by galvanostatic charge discharge at 10 A g^{-1}. Inset: galvanostatic charge–discharge profiles.[151]

modifications of the bond strength of metal-ligand structural units may address these issues. In future studies, theoretical prediction based on computational modelling might significantly aid the design and discovery of new optimal MOFs for energy storage applications. Thus, 2D inherently conductive MOFs are promising alternatives electrodes for electrical-double layer capacitors and pseudo-capacitors.

Electrochemically-controlled capture and release

Electrochemical transformations offer potential advantages over other catalytic methods due to their mild conditions, minimal waste, and potential for energy-efficiency. Amongst other 2D materials, MOFs are very unique since they are capable of bridging the areas of homogeneous and heterogeneous catalysis by harnessing many of the advantageous qualities of both systems.[183] Such modularly prepared 2D MOF structures can induce the stability of heterogeneous catalysts and preserve the well-defined molecular catalytic units found in homogeneous systems.[184] 2D conductive MOFs can be thus envisioned as new generation of nanomaterials for catalysis because of their highly ordered and tailorable pores or channels, which can provide a suitable confined environment for catalysing reactions with appropriate size-selectivity, as well as provide an ordered distribution of highly dense analyte-accessible active sites throughout the MOF framework. Moreover, high density of incorporated catalytic sites can offer increased reaction rates which are not often accessible using conventional 2D materials. Further improvements in turnover rates can arise from the ordered arrangement of pores in the MOFs frameworks that permits efficient diffusion of reactants and products out of the solid material, which leads to increased efficiency of catalytic reactions.[185]

We harnessed the multifunctional nature of 2D MOFs combining redox activity and the presence of reactive metal bis(dithiolene) active sites for voltage-actuated reversible capture of ethylene. This concept was demonstrated using M_3HTTP_2 porous coordination polymers (PCPs, M = Co, Ni and Cu) that were highly amorphous in character with certain features of MOFs such as large surface area and good thermal stability.[152] These conductive PCPs were then incorporated into solid-state devices through either mechanical compressions into pellets or by drop-casting aliquots of each MOF onto gold-plated electrodes (**Figure 11**).[152] Applying a positive bias (+2.0 V) to the M_3HTTP_2 promoted capture of ethylene. The

subsequent delivery of negative potential (−2.0 V) induced its release. The amounts of electrochemically captured ethylene for drop-cast MOF thin films (3 – 6 mg/g) was approximately time times larger than recorded for compressed pellets (0.1 – 0.5 mg/g) suggesting that the exposed surface area dominated the capture process. These materials also exhibited high resistance to common interfering agents such as CO and H_2S, and retained
at least 50% of their function after the exposure to 2 ppt of both interferants. Although, more detailed computational and experimental investigations of the mechanism of ethylene binding to the MOF is required, we suggested that ethylene interactions with the metal bis(dithiolene) moiety within the framework may proceed through a cycloaddition reaction, as reported for molecular complexes.[186]

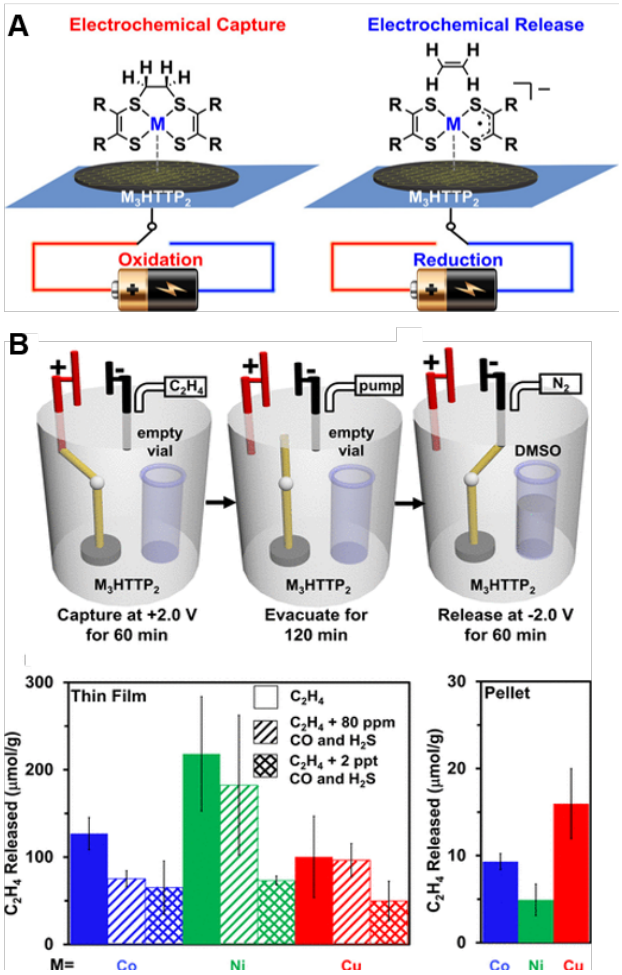

Figure 11. A) Synthesis of PCPs. Illustration of proposed voltage-actuated capture and release of ethylene with PCPs. B) Experimental design and demonstration for solid-state electrochemical capture and release of ethylene. The setup comprises the PCPs positioned under ethylene atmosphere (~1 atm) in a sealed container. Applied electrical potential (+2.0 V) to the material facilitates ethylene capture. Switching off the power and evacuating at 1.5×10^{-3} Torr removes all unbound ethylene. Refilling of the container with N_2, and addition of deuterated dimethyl sulfoxide (DMSO-d_6) enables monitoring of electrochemical release by NMR. Subsequent reduction at −2.0 V promotes ethylene release. The amount of ethylene quantified in the electrochemical capture/release experiment in the absence and presence of interferents (80 ppm and 2 ppt of CO and H_2S) by thin films and pellets.[152]

Conclusions and Outlook

2D conductive MOFs are poised for the development of next generation of technologies due to their unique features and multifunctional character. The access to MOFs with new and often tuneable electronic properties opened up a new class of conductive materials that combined unique capabilities emergent from the distinct nature of the structural building blocks that comprise them. These developments in material research have the potential to elevate 2D conductive MOFs above the level of other 2D materials due to their entirely different mechanical, structural, electrical, and chemical properties which can be readily modulated and accessed through modular synthesis from an almost unlimited number of structurally distinct molecular building units. In this review, we highlighted some of the more recent progress in understanding the structural properties of 2D conductive MOFs that dictate and ultimately lead to their intrinsic electrical conductivity. We also demonstrated numerous applied areas in which 2D conductive MOFs are likely to surpass other 2D materials including sensor development, energy storage devices, and catalysis. The current challenges and opportunities in such applications demonstrate the continually expanding interest in the development of 2D conductive MOFs.

The electronic, chemical and physical properties of 2D conductive MOFs are defined by their structural features, which further define the performance of these materials in practical applications. However, harnessing the full potential of these structural features through functional performance requires several fundamental scientific advances in 2D MOF research. *First*, controlled synthesis of 2D conductive MOFs with predictable and desired structures remains difficult to achieve using available synthetic methods. Therefore, the preparation of ultrathin epitaxially oriented 2D nanomaterials with desired structural characteristics in a highly controllable manner is still one of the major challenges in this field. Additionally, the ability to produce and characterize single-crystals of layered 2D MOFs remains an unresolved challenge. *Second*, the molecular engineered of targeted structure-property relationships remains difficult due to limited fundamental understanding of intrinsic MOF structure and limited knowledge of host-guest interactions within MOFs. Overcome this challenge will require rigorous computational modelling combined with spectroscopic assessment of MOF surfaces. *Third*, even when the first two challenges are resolved, interfacing MOFs with electrodes within functional devices will remain an important aspect influencing their performance characteristics as functional materials. Ideally, this issue could be addressed by improving the current methods of direct self-assembly of 2D conductive MOFs onto the functional devices. Given that the electrically conductive, multifunctional 2D MOFs have already demonstrated excellent performance in numerous applications, the ultimate goal is to enable the design of the materials with predictable and targeted structure-property relationship that could address and overcome current limitations of other materials and surpass their performance.

Conflicts of interest

There are no conflicts to declare.

Acknowledgements

The authors acknowledge support from start-up funds provided by Dartmouth College, from Walter and Constance Burke Research Initiation Award, and from the Army Research Office Young Investigator Program Grant No. W911NF-17-1-0398.

Notes and references

1. H. Zhang, *ACS Nano*, 2015, **9**, 9451-9469.
2. C. Tan, X. Cao, X. J. Wu, Q. He, J. Yang, X. Zhang, J. Chen, W. Zhao, S. Han, G. H. Nam, M. Sindoro and H. Zhang, *Chem. Rev.*, 2017, **117**, 6225-6331.
3. A. K. Geim and K. S. Novoselov, *Nat. Mater.*, 2007, **6**, 183-191.
4. A. Gupta, T. Sakthivel and S. Seal, *Prog. Mater Sci.*, 2015, **73**, 44-126.
5. K. S. Novoselov, A. K. Geim, S. V. Morozov, D. Jiang, Y. Zhang, S. V. Dubonos, I. V. Grigorieva and A. A. Firsov, *Science (New York, N.Y.)*, 2004, **306**, 666-669.
6. C. Tan and H. Zhang, *Chem. Soc. Rev.*, 2015, **44**, 2713-2731.
7. M. Chhowalla, H. S. Shin, G. Eda, L. J. Li, K. P. Loh and H. Zhang, *Nat. Chem.*, 2013, **5**, 263-275.
8. X. Huang, Z. Zeng and H. Zhang, *Chem. Soc. Rev.*, 2013, **42**, 1934-1946.
9. R. Lv, J. A. Robinson, R. E. Schaak, D. Sun, Y. Sun, T. E. Mallouk and M. Terrones, *Acc. Chem. Res.*, 2015, **48**, 56-64.
10. C. Tan and H. Zhang, *Nat. Commun.*, 2015, **6**, 7873.
11. W. J. Ong, L. L. Tan, Y. H. Ng, S. T. Yong and S. P. Chai, *Chem. Rev.*, 2016, **116**, 7159-7329.
12. L. H. Li and Y. Chen, *Adv. Func. Mater.*, 2016, **26**, 2594-2608.
13. Q. Weng, X. Wang, X. Wang, Y. Bando and D. Golberg, *Chem. Soc. Rev.*, 2016, **45**, 3989-4012.
14. Y. Lin, T. V. Williams and J. W. Connell, *J. Phys. Chem. Lett.*, 2009, **237**, 277-283.
15. M. Naguib, V. N. Mochalin, M. W. Barsoum and Y. Gogotsi, *Adv. Mater.*, 2014, **26**, 992-1005.
16. R. Ma and T. Sasaki, *Acc. Chem. Res.*, 2015, **48**, 136-143.
17. M. Osada and T. Sasaki, *J. Mater. Chem.*, 2009, **19**, 2503-2511.
18. H. Duan, N. Yan, R. Yu, C. R. Chang, G. Zhou, H. S. Hu, H. Rong, Z. Niu, J. Mao, H. Asakura, T. Tanaka, P. J. Dyson, J. Li and Y. Li, *Nat. Commun.*, 2014, **5**, 3093.
19. J. Niu, D. Wang, H. Qin, X. Xiong, P. Tan, Y. Li, R. Liu, X. Lu, J. Wu, T. Zhang, W. Ni and J. Jin, *Nat. Commun.*, 2014, **5**, 3313.
20. O. M. Yaghi and H. L. Li, *J. Am. Chem. Soc.*, 1995, **117**, 10401-10402.
21. Q. Wang and D. O'Hare, *Chem. Rev.*, 2012, **112**, 4124-4155.
22. J. Shamsi, Z. Dang, P. Bianchini, C. Canale, F. D. Stasio, R. Brescia, M. Prato and L. Manna, *J. Am. Chem. Soc.*, 2016, **138**, 7240-7243.
23. J. Song, L. Xu, J. Li, J. Xue, Y. Dong, X. Li and H. Zeng, *Adv. Mater.*, 2016, **28**, 4861-4869.
24. S. Demirci, N. Avazli, E. Durgun and S. Cahangirov, *Phys. Rev. B*, 2017, **95**.
25. W. C. Yap, Z. Yang, M. Mehboudi, J.-A. Yan, S. Barraza-Lopez and W. Zhu, *Nano Ress*, 2017, **11**, 420-430.
26. Y. Peng, Y. Li, Y. Ban and W. Yang, *Angew. Chem. Int. Ed. Engl.*, 2017, **56**, 9757-9761.
27. J. C. Tan, P. J. Saines, E. G. Bithell and A. K. Cheetham, *ACS Nano*, 2012, **6**, 615-621.
28. G. S. Papaefstathiou, T. Friscic and L. R. MacGillivray, *J. Am. Chem. Soc.*, 2005, **127**, 14160-14161.
29. V. Eswaraiah, Q. Zeng, Y. Long and Z. Liu, *Small*, 2016, **12**, 3480-3502.
30. H. Liu, Y. Du, Y. Deng and P. D. Ye, *Chem. Soc. Rev.*, 2015, **44**, 2732-2743.
31. M. M. Khin, A. S. Nair, V. J. Babu, R. Murugan and S. Ramakrishna, *Energ Environ Sci*, 2012, **5**, 8075-8109.
32. M. S. Mauter and M. Elimelech, *Environ. Sci. Technol.*, 2008, **42**, 5843-5859.
33. F. Perreault, A. Fonseca de Faria and M. Elimelech, *Chem. Soc. Rev.*, 2015, **44**, 5861-5896.
34. Z. Wang and B. Mi, *Environ. Sci. Technol.*, 2017, **51**, 8229-8244.
35. D. Chimene, D. L. Alge and A. K. Gaharwar, *Adv. Mater.*, 2015, **27**, 7261-7284.
36. Y. Chen, C. Tan, H. Zhang and L. Wang, *Chem. Soc. Rev.*, 2015, **44**, 2681-2701.
37. D. L. Duong, S. J. Yun and Y. H. Lee, *ACS Nano*, 2017, **11**, 11803-11830.
38. Z. Cai, B. Liu, X. Zou and H. M. Cheng, *Chem. Rev.*, 2018, DOI: 10.1021/acs.chemrev.7b00536.
39. Y. Sun, S. Gao and Y. Xie, *Chem. Soc. Rev.*, 2014, **43**, 530-546.
40. X. Zhang and Y. Xie, *Chem. Soc. Rev.*, 2013, **42**, 8187-8199.
41. D. Voiry, J. Yang and M. Chhowalla, *Adv. Mater.*, 2016, **28**, 6197-6206.
42. M. D. Stoller, S. Park, Y. Zhu, J. An and R. S. Ruoff, *Nano Lett.*, 2008, **8**, 3498-3502.
43. K. J. Koski and Y. Cui, *ACS Nano*, 2013, **7**, 3739-3743.
44. X. Guo, X. Zhang, S. Zhao, Q. Huang and J. Xue, *Phys. Chem. Chem. Phys.*, 2016, **18**, 228-233.
45. W. Choi, N. Choudhary, G. H. Han, J. Park, D. Akinwande and Y. H. Lee, *Mater. Today*, 2017, **20**, 116-130.
46. N. Huang, X. Chen, R. Krishna and D. L. Jiang, *Angew. Chem. Int. Ed. Engl.*, 2015, **54**, 2986-2990.
47. M. Yi and Z. G. Shen, *J. M.Chem. A*, 2015, **3**, 11700-11715.
48. S. Achmann, G. Hagen, J. Kita, I. M. Malkowsky, C. Kiener and R. Moos, *Sensors* 2009, **9**, 1574-1589.
49. Z. Zeng, Z. Yin, X. Huang, H. Li, Q. He, G. Lu, F. Boey and H. Zhang, *Angew. Chem. Int. Ed. Engl.*, 2011, **50**, 11093-11097.
50. W. S. Hummers and R. E. Offeman, *J. Am. Chem. Soc.*, 1958, **80**, 1339-1339.
51. M. Naguib, O. Mashtalir, J. Carle, V. Presser, J. Lu, L. Hultman, Y. Gogotsi and M. W. Barsoum, *ACS Nano*, 2012, **6**, 1322-1331.
52. J. X. Yu, J. Li, W. F. Zhang and H. X. Chang, *Chem. Sci.*, 2015, **6**, 6705-6716.
53. P. Z. Li, Y. Maeda and Q. Xu, *ChemComm*, 2011, **47**, 8436-8438.
54. Y. Huang, E. Sutter, N. N. Shi, J. Zheng, T. Yang, D. Englund, H. J. Gao and P. Sutter, *ACS Nano*, 2015, **9**, 10612-10620.

55. K. K. Liu, W. Zhang, Y. H. Lee, Y. C. Lin, M. T. Chang, C. Y. Su, C. S. Chang, H. Li, Y. Shi, H. Zhang, C. S. Lai and L. J. Li, *Nano Lett.*, 2012, **12**, 1538-1544.
56. M. Zhao, Q. Lu, Q. Ma and H. Zhang, *Small Methods*, 2017, **1**.
57. K. K. Tanabe and S. M. Cohen, *Chem. Soc. Rev.*, 2011, **40**, 498-519.
58. I. Stassen, N. Burtch, A. Talin, P. Falcaro, M. Allendorf and R. Ameloot, *Chem. Soc. Rev.*, 2017, **46**, 3185-3241.
59. D. M. D'Alessandro, J. R. R. Kanga and J. S. Caddy, *Aust. J. Chem.*, 2011, **64**, 718-722.
60. M. D. Allendorf, A. Schwartzberg, V. Stavila and A. A. Talin, *Chem. Eur. J.*, 2011, **17**, 11372-11388.
61. V. Stavila, A. A. Talin and M. D. Allendorf, *Chem. Soc. Rev.*, 2014, **43**, 5994-6010.
62. T. Y. Ma, S. Dai, M. Jaroniec and S. Z. Qiao, *J. Am. Chem. Soc.*, 2014, **136**, 13925-13931.
63. A. J. Clough, J. W. Yoo, M. H. Mecklenburg and S. C. Marinescu, *J. Am. Chem. Soc.*, 2015, **137**, 118-121.
64. H. Li, M. Eddaoudi, M. O'Keeffe and O. M. Yaghi, *Nature*, 1999, **402**, 276-279.
65. D. Sheberla, J. C. Bachman, J. S. Elias, C. J. Sun, Y. Shao-Horn and M. Dincă, *Nat. Mater.*, 2017, **16**, 220-224.
66. Y. Zhao, Z. X. Song, X. Li, Q. Sun, N. C. Cheng, S. Lawes and X. L. Sun, *Energy Storage Mater*, 2016, **2**, 35-62.
67. M. G. Campbell, D. Sheberla, S. F. Liu, T. M. Swager and M. Dincă, *Angew. Chem. Int. Ed. Engl.*, 2015, **54**, 4349-4352.
68. M. K. Smith, K. E. Jensen, P. A. Pivak and K. A. Mirica, *Chem. Mater.*, 2016, **28**, 5264-5268.
69. A. A. Talin, A. Centrone, A. C. Ford, M. E. Foster, V. Stavila, P. Haney, R. A. Kinney, V. Szalai, F. El Gabaly, H. P. Yoon, F. Leonard and M. D. Allendorf, *Science (New York, N.Y.)*, 2014, **343**, 66-69.
70. L. Sun, M. G. Campbell and M. Dincă, *Angew. Chem. Int. Ed. Engl.*, 2016, **55**, 3566-3579.
71. Z. Shuai, L. Wang and C. Song, *Theory of Charge Transport in Carbon Electronic Materials*, Springer Berlin Heidelberg, 2012.
72. A. G. MacDiarmid, *Angew. Chem. Int. Ed.*, 2001, **40**, 2581-2590.
73. S. Hideki, *Angew. Chem. Int. Ed.*, 2001, **40**, 2574-2580.
74. A. J. Heeger, *Angew. Chem. Int. Ed.*, 2001, **40**, 2591-2611.
75. J. Ferraris, D. O. Cowan, V. Walatka and J. H. Perlstein, *J. Am. Chem. Soc.*, 1973, **95**, 948-949.
76. R. M. Laine, *Inorganic and Organometallic Polymers with Special Properties*, Springer Netherlands, 2012.
77. S. E. Harrison and K. H. Ludewig, *J. Chem. Phys.*, 1966, **45**, 343-348.
78. G. Givaja, P. Amo-Ochoa, C. J. Gomez-Garcia and F. Zamora, *Chem. Soc. Rev.*, 2012, **41**, 115-147.
79. S. R. Batten, S. M. Neville and D. R. Turner, *Coordination Polymers: Design, Analysis and Application*, Royal Society of Chemistry, 2008.
80. M. J. Allen, V. C. Tung and R. B. Kaner, *Chem. Rev.*, 2010, **110**, 132-145.
81. K. I. Bolotin, K. J. Sikes, Z. Jiang, M. Klima, G. Fudenberg, J. Hone, P. Kim and H. L. Stormer, *Solid State Commun.*, 2008, **146**, 351-355.
82. R. L. McCreery, *Chem. Rev.*, 2008, **108**, 2646-2687.
83. A. H. Castro Neto, F. Guinea, N. M. R. Peres, K. S. Novoselov and A. K. Geim, *Rev. Mod. Phys.*, 2009, **81**, 109-162.
84. E. M. Kiarii, K. K. Govender, P. G. Ndungu and P. P. Govender, *Chem. Phys. Lett.*, 2017, **678**, 167-176.
85. K. Vandewal, S. Albrecht, E. T. Hoke, K. R. Graham, J. Widmer, J. D. Douglas, M. Schubert, W. R. Mateker, J. T. Bloking, G. F. Burkhard, A. Sellinger, J. M. Frechet, A. Amassian, M. K. Riede, M. D. McGehee, D. Neher and A. Salleo, *Nat. Mater.*, 2014, **13**, 63-68.
86. J. Singh, *Semiconductor Devices : Basic Principles*, Wiley India Pvt. Limited, 2007.
87. N. Karl, *Synth. Met.*, 2003, **133-134**, 649-657.
88. R. Enderlein and N. J. M. Horing, *Fundamentals of Semiconductor Physics and Devices*, World Scientific, 1997.
89. Q. A. Acton, *Advances in Carbon Research and Application*, ScholarlyEditions, 2013.
90. M. Schwoerer and H. C. Wolf, *Organic Molecular Solids*, Wiley, 2008.
91. O. N. B. Sundaram, *Thin Film Techniques and Applications*, Allied Publishers, 2004.
92. C. H. Hendon, D. Tiana and A. Walsh, *Phys. Chem. Chem. Phys.*, 2012, **14**, 13120-13132.
93. D. M. D'Alessandro, *Chem. Commun.*, 2016, **52**, 8957-8971.
94. A. Walsh, K. T. Butler and C. H. Hendon, *MRS Bull.*, 2016, **41**, 870-876.
95. C. F. Leong, P. M. Usov and D. M. D'Alessandro, *MRS Bull.*, 2016, **41**, 858-864.
96. M. Dincă and F. Léonard, *MRS Bull.*, 2016, **41**, 854-857.
97. T. Neumann, J. Liu, T. Wachter, P. Friederich, F. Symalla, A. Welle, V. Mugnaini, V. Meded, M. Zharnikov, C. Woll and W. Wenzel, *ACS Nano*, 2016, **10**, 7085-7093.
98. C. A. Allen and S. M. Cohen, *Inorg. Chem.*, 2014, **53**, 7014-7019.
99. M. G. Campbell and M. Dincă, *Sensors* 2017, **17**.
100. J. R. Winkler and H. B. Gray, *J. Am. Chem. Soc.*, 2014, **136**, 2930-2939.
101. M. Pollak and B. Shklovskii, *Hopping Transport in Solids*, Elsevier Science, 1991.
102. T. C. Narayan, T. Miyakai, S. Seki and M. Dincă, *J. Am. Chem. Soc.*, 2012, **134**, 12932-12935.
103. S. S. Park, E. R. Hontz, L. Sun, C. H. Hendon, A. Walsh, T. Van Voorhis and M. Dincă, *J. Am. Chem. Soc.*, 2015, **137**, 1774-1777.
104. S. Takaishi, M. Hosoda, T. Kajiwara, H. Miyasaka, M. Yamashita, Y. Nakanishi, Y. Kitagawa, K. Yamaguchi, A. Kobayashi and H. Kitagawa, *Inorg. Chem.*, 2009, **48**, 9048-9050.
105. Y. Kobayashi, B. Jacobs, M. D. Allendorf and J. R. Long, *Chem. Mater.*, 2010, **22**, 4120-4122.
106. J. Singleton, *Band Theory and Electronic Properties of Solids*, OUP Oxford, 2001.
107. D. Long, *Energy bands in semiconductors*, Interscience Publishers, 1968.
108. H. V. Keer, *Principles of the Solid State*, J. Wiley & Sons, 1993.
109. S. Luryi, B. I. Shklovskii and A. L. Efros, *Electronic Properties of Doped Semiconductors*, Springer Berlin Heidelberg, 2013.
110. P. Stallinga, *Adv. Mater.*, 2011, **23**, 3356-3362.
111. L. Sun, C. H. Hendon, M. A. Minier, A. Walsh and M. Dincă, *J. Am. Chem. Soc.*, 2015, **137**, 6164-6167.
112. Q. Zhang, B. Li and L. Chen, *Inorg. Chem.*, 2013, **52**, 9356-9362.

113. D. S. Seferos, S. A. Trammell, G. C. Bazan and J. G. Kushmerick, *Proc. Natl. Acad. Sci. U. S. A.*, 2005, **102**, 8821-8825.
114. I. Ciofini, T. Le Bahers, C. Adamo, F. Odobel and D. Jacquemin, *J. Phys. Chem. C*, 2012, **116**, 11946-11955.
115. R. Hoffmann, *Acc. Chem. Res.*, 2002, **4**, 1-9.
116. F. Gándara, N. Snejko, A. d. Andrés, J. R. Fernandez, J. C. Gómez-Sal, E. Gutierrez-Puebla and A. Monge, *RSC Adv.*, 2012, **2**, 949-955.
117. M. Shengqian and P. J. A, *Elaboration And Applications Of Metal-organic Frameworks*, World Scientific Publishing Company, 2018.
118. J. L. Atwood, G. W. Gokel and L. Barbour, *Comprehensive Supramolecular Chemistry II*, Elsevier Science, 2017.
119. M. Dincă and F. Léonard, *MRS Bulletin*, 2016, **41**, 854-857.
120. Z. Bao and J. Locklin, *Organic Field-Effect Transistors*, CRC Press, 2007.
121. L.-P. Tang, L.-M. Tang, H. Geng, Y.-P. Yi, Z. Wei, K.-Q. Chen and H.-X. Deng, *Appl. Phys. Lett.*, 2018, **112**, 012101.
122. D. Sheberla, L. Sun, M. A. Blood-Forsythe, S. Er, C. R. Wade, C. K. Brozek, A. Aspuru-Guzik and M. Dincă, *J. Am. Chem. Soc.*, 2014, **136**, 8859-8862.
123. M. Hmadeh, Z. Lu, Z. Liu, F. Gandara, H. Furukawa, S. Wan, V. Augustyn, R. Chang, L. Liao, F. Zhou, E. Perre, V. Ozolins, K. Suenaga, X. F. Duan, B. Dunn, Y. Yamamto, O. Terasaki and O. M. Yaghi, *Chem. Mater.* , 2012, **24**, 3511-3513.
124. J. H. Dou, L. Sun, Y. Ge, W. Li, C. H. Hendon, J. Li, S. Gul, J. Yano, E. A. Stach and M. Dincă, *J. Am. Chem. Soc.*, 2017, **139**, 13608-13611.
125. A. J. Clough, J. M. Skelton, C. A. Downes, A. A. de la Rosa, J. W. Yoo, A. Walsh, B. C. Melot and S. C. Marinescu, *J. Am. Chem. Soc.*, 2017, **139**, 10863-10867.
126. Z. Lin, A. McCreary, N. Briggs, S. Subramanian, K. Zhang, Y. Sun, X. Li, N. J. Borys, H. Yuan, S. K. Fullerton-Shirey, A. Chernikov, H. Zhao, S. McDonnell, A. M. Lindenberg, K. Xiao, B. J. LeRoy, M. Drndić, J. C. M. Hwang, J. Park, M. Chhowalla, R. E. Schaak, A. Javey, M. C. Hersam, J. Robinson and M. Terrones, *2D Materials*, 2016, **3**.
127. C. H. Hendon, A. J. Rieth, M. D. Korzynski and M. Dincă, *ACS Cent. Sci.*, 2017, **3**, 554-563.
128. C. K. Brozek and M. Dincă, *J. Am. Chem. Soc.*, 2013, **135**, 12886-12891.
129. M. A. Nasalevich, C. H. Hendon, J. G. Santaclara, K. Svane, B. van der Linden, S. L. Veber, M. V. Fedin, A. J. Houtepen, M. A. van der Veen, F. Kapteijn, A. Walsh and J. Gascon, *Sci. Rep.*, 2016, **6**, 23676.
130. M. Ko, A. Aykanat, M. K. Smith and K. A. Mirica, *Sensors* 2017, **17**.
131. M. K. Smith and K. A. Mirica, *J. Am. Chem. Soc.*, 2017, **139**, 16759-16767.
132. C. S. Grange, A. J. Meijer and M. D. Ward, *Dalton Trans.*, 2010, **39**, 200-211.
133. M. E. Foster, K. Sohlberg, M. D. Allendorf and A. A. Talin, *J. Phys. Chem. Lett.*, 2018, **9**, 481-486.
134. S. Chen, J. Dai and X. C. Zeng, *Phys. Chem. Chem. Phys.*, 2015, **17**, 5954-5958.
135. M. Bosch, S. Yuan, W. Rutledge and H. C. Zhou, *Acc. Chem. Res.*, 2017, **50**, 857-865.
136. W. Shi, S. Song and H. Zhang, *Chem. Soc. Rev.*, 2013, **42**, 5714-5743.
137. L. E. Darago, M. L. Aubrey, C. J. Yu, M. I. Gonzalez and J. R. Long, *J. Am. Chem. Soc.*, 2015, **137**, 15703-15711.
138. T. Kambe, R. Sakamoto, K. Hoshiko, K. Takada, M. Miyachi, J. H. Ryu, S. Sasaki, J. Kim, K. Nakazato, M. Takata and H. Nishihara, *J. Am. Chem. Soc.*, 2013, **135**, 2462-2465.
139. R. Dong, M. Pfeffermann, H. Liang, Z. Zheng, X. Zhu, J. Zhang and X. Feng, *Angew. Chem. Int. Ed. Engl.*, 2015, **54**, 12058-12063.
140. J. Cui and Z. Xu, *ChemComm*, 2014, **50**, 3986-3988.
141. H. Jia, Y. Yao, J. Zhao, Y. Gao, Z. Luo and P. Du, *J. Mater. Chem. A*, 2018, **6**, 1188-1195.
142. N. Lahiri, N. Lotfizadeh, R. Tsuchikawa, V. V. Deshpande and J. Louie, *J. Am. Chem. Soc.*, 2017, **139**, 19-22.
143. M. S. Yao, X. J. Lv, Z. H. Fu, W. H. Li, W. H. Deng, G. D. Wu and G. Xu, *Angew. Chem. Int. Ed. Engl.*, 2017, **56**, 16510-16514.
144. M. G. Campbell, S. F. Liu, T. M. Swager and M. Dincă, *J. Am. Chem. Soc.*, 2015, **137**, 13780-13783.
145. L. Mendecki and K. A. Mirica, *ACS Appl. Mater. Interfaces*, 2018. DOI: 10.1021/acsami.8b03956
146. C. A. Downes, A. J. Clough, K. Chen, J. W. Yoo and S. C. Marinescu, *ACS Appl. Mater. Interfaces*, 2018, **10**, 1719-1727.
147. X. Huang, H. Yao, Y. Cui, W. Hao, J. Zhu, W. Xu and D. Zhu, *ACS Appl. Mater. Interfaces*, 2017, **9**, 40752-40759.
148. X. Sun, K. H. Wu, R. Sakamoto, T. Kusamoto, H. Maeda, X. Ni, W. Jiang, F. Liu, S. Sasaki, H. Masunaga and H. Nishihara, *Chem. Sci.*, 2017, **8**, 8078-8085.
149. E. M. Miner, T. Fukushima, D. Sheberla, L. Sun, Y. Surendranath and M. Dincă, *Nat. Commun.*, 2016, **7**, 10942.
150. W.-H. Li, K. Ding, H.-R. Tian, M.-S. Yao, B. Nath, W.-H. Deng, Y. Wang and G. Xu, *Adv. Func. Mater.*, 2017, **27**.
151. D. Feng, T. Lei, M. R. Lukatskaya, J. Park, Z. Huang, M. Lee, L. Shaw, S. Chen, A. A. Yakovenko, A. Kulkarni, J. Xiao, K. Fredrickson, J. B. Tok, X. Zou, Y. Cui and Z. Bao, *Nat. Energy*, 2018, **3**, 30-36.
152. L. Mendecki, M. Ko, X. Zhang, Z. Meng and K. A. Mirica, *J. Am. Chem. Soc.*, 2017, **139**, 17229-17232.
153. G. Wu, J. Huang, Y. Zang, J. He and G. Xu, *J. Am. Chem. Soc.*, 2017, **139**, 1360-1363.
154. X. Huang, P. Sheng, Z. Tu, F. Zhang, J. Wang, H. Geng, Y. Zou, C. A. Di, Y. Yi, Y. Sun, W. Xu and D. Zhu, *Nat. Commun.*, 2015, **6**, 7408.
155. M. E. Ziebel, L. E. Darago and J. R. Long, *J. Am. Chem. Soc.*, 2018, **140**, 3040-3051.
156. W. Li, L. Sun, J. Qi, P. Jarillo-Herrero, M. Dincă and J. Li, *Chem. Sci.*, 2017, **8**, 2859-2867.
157. Y. Liu, X. Zhao, B. Cai, T. Pei, Y. Tong, Q. Tang and Y. Liu, *Nanoscale*, 2014, **6**, 1323-1328.
158. Y. Peng, Y. Li, Y. Ban, H. Jin, W. Jiao, X. Liu and W. Yang, *Science (New York, N.Y.)*, 2014, **346**, 1356-1359.
159. P. J. Saines, J. C. Tan, H. H. Yeung, P. T. Barton and A. K. Cheetham, *Dalton Trans.*, 2012, **41**, 8585-8593.
160. C. Hermosa, B. R. Horrocks, J. I. Martinez, F. Liscio, J. Gomez-Herrero and F. Zamora, *Chem. Sci.*, 2015, **6**, 2553-2558.
161. P. J. Saines, M. Steinmann, J. C. Tan, H. H. Yeung, W. Li, P. T. Barton and A. K. Cheetham, *Inorg. Chem.*, 2012, **51**, 11198-11209.
162. O. M. Yaghi, *J. Am. Chem. Soc.*, 2016, **138**, 15507-15509.
163. O. M. Yaghi, M. O'Keeffe, N. W. Ockwig, H. K. Chae, M. Eddaoudi and J. Kim, *Nature*, 2003, **423**, 705-714.

164. V. Rubio-Gimenez, M. Galbiati, J. Castells-Gil, N. Almora-Barrios, J. Navarro-Sanchez, G. Escorcia-Ariza, M. Mattera, T. Arnold, J. Rawle, S. Tatay, E. Coronado and C. Marti-Gastaldo, *Adv. Mater.*, 2018, **30**.
165. W. H. Li, K. Ding, H. R. Tian, M. S. Yao, B. Nath, W. H. Deng, Y. B. Wang and G. Xu, *Adv. Funct. Mater.*, 2017, **27**, 1702067.
166. E. M. Miner and M. Dincă, *Nat. Energy*, 2016, **1**, 16186.
167. N. Stock and S. Biswas, *Chem. Rev.*, 2012, **112**, 933-969.
168. J. W. Matthews, *Epitaxial growth*, Academic Press, New York, 1975.
169. H. Gliemann and C. Wöll, *Mater. Today*, 2012, **15**, 110-116.
170. Z.-G. Gu and J. Zhang, *Coord. Chem. Rev.*, 2017, DOI: 10.1016/j.ccr.2017.09.028.
171. C. L. Tan, J. Z. Chen, X. J. Wu and H. Zhang, *Nat. Rev. Mater.*, 2018, **3**, 17089.
172. B. Li, H. M. Wen, Y. Cui, W. Zhou, G. Qian and B. Chen, *Adv. Mater.*, 2016, **28**, 8819-8860.
173. M. K. Smith, S. R. Angle and B. H. Northrop, *J. Chem. Educ.*, 2014, **92**, 368-372.
174. K. Sumida and J. Arnold, *J. Chem. Educ.*, 2011, **88**, 92-94.
175. T.-H. Le, Y. Kim and H. Yoon, *Polymers*, 2017, **9**, 150.
176. M. E. Foster, K. Sohlberg, C. D. Spataru and M. D. Allendorf, *J. Phys. Chem. C*, 2016, **120**, 15001-15008.
177. Y. Abghoui and E. Skulason, *J. Phys. Chem. C*, 2017, **121**, 24036-24045.
178. C. A. Downes and S. C. Marinescu, *ChemSusChem*, 2017, **10**, 4374-4392.
179. H. Wang, Q.-L. Zhu, R. Zou and Q. Xu, *Chem*, 2017, **2**, 52-80.
180. S. Zhao, Y. Wang, J. Dong, C.-T. He, H. Yin, P. An, K. Zhao, X. Zhang, C. Gao, L. Zhang, J. Lv, J. Wang, J. Zhang, A. M. Khattak, N. A. Khan, Z. Wei, J. Zhang, S. Liu, H. Zhao and Z. Tang, *Nat. Energy*, 2016, **1**.
181. G. Y. Xu, P. Nie, H. Dou, B. Ding, L. Y. Li and X. G. Zhang, *Mater. Today*, 2017, **20**, 191-209.
182. J. R. Miller and P. Simon, *Science (New York, N.Y.)*, 2008, **321**, 651-652.
183. L. Zhu, X. Q. Liu, H. L. Jiang and L. B. Sun, *Chem. Rev.*, 2017, **117**, 8129-8176.
184. C. J. Doonan and C. J. Sumby, *CrystEngComm*, 2017, **19**, 4044-4048.
185. J. Liu, L. Chen, H. Cui, J. Zhang, L. Zhang and C. Y. Su, *Chem. Soc. Rev.*, 2014, **43**, 6011-6061.
186. K. Wang and E. I. Stiefel, *Science (New York, N.Y.)*, 2001, **291**, 106-109.